Investigation and Analysis of Thermal Performance of InGaN/GaN Light Emitting Diodes

by

Shiladitya Das

A Thesis Presented in Partial Fulfilment
of the Requirements for the Degree
Master of Science

Approved September 2017 by the
Graduate Supervisory Committee:

Yuji Zhao, Chair
Dragica Vasileska
Cun Zheng Ning

ARIZONA STATE UNIVERSITY

December 2017

ABSTRACT

Light Emitting Diodes even with their longer life, robust build and low power consumption, they are still plagued by some problems the most significant of which are the current droop and thermal droop. Current droop causes a lowering in the Internal Quantum Efficiency with increased current injection while thermal droop lowers the whole Internal Quantum Efficiency curve with increase in temperature. The focus here was understanding effects of thermal droop and develop a method to control it.

Shockley Read Hall recombination plays a dominant role in the thermal droop effect when the current injection is low. Since the blue light emitting diode is based on Gallium Nitride, we need to take into consideration the effect of piezoelectric polarization in the quantum wells. The effects of the piezoelectric fields were studied based on the Gallium Nitride plane orientations. It was found in a Gallium Nitride light emitting diodes simulation study that more the number of quantum wells, lower would be the Radiative recombination rate. The problem of exacerbated spatial separation of electron hole wavefunctions in a thick single quantum well structure lead to the development of a dual well structure where one well assisted the other during high temperature operations. The Electron Blocking Layer was reduced in thickness and was made only 10 nm thick with a 5 nm Gallium Nitride buffer between it and the active region wells. The main reason for reducing the electron blocking layer thickness was to reduce the valance band offset and improve hole transport into the active region. Three different dual well designs were simulated of 3nm, 6nm and 9nm wide wells. The output parameters like the Power Spectral Density, Electron bound density, Light Output Power and Electron-Hole wavefunction overlaps were calculated. It was found

that one of the wells acted as an assisting well where it had very little radiative recombination activity in it at room temperature.

As the temperature increased, it was observed that the electrons in the main well started to overflow out of it and into the assisting well where the radiative recombination rate increased significantly. This lead to a boost in Internal Quantum Efficiency.

ACKNOWLEDGMENTS

I would like to convey my gratitude to my advisor Prof Yuji Zhao for guiding me through this research work. His profound understanding of optoelectronics and valuable advice helped me understand this field better that aided tremendously in my research.

My parents Dr Tania Dass and Dr Tapan Kumar Dass have always been by my side like pillars to support me and push me ahead.

I would like to take this opportunity to thank my classmates Vishwanathan Naveen Kumar and Marut Pattanaik to help me push forward in this research to give it form and substance.

TABLE OF CONTENTS

PAGE

CHAPTER PAGE

Appendix PAGE

LIST OF FIGURES

Figure Page

Figure Page

Figure Page

LIST OF TABLES

Table Page

INTRODUCTION

1.1 Present Scenario

LED lighting technology is quickly becoming the dominant source of lighting in the modern world. The numerous advantages that solid-state lighting technology possesses over conventional incandescent light bulbs or CFLs like much lower electrical power consumption, longer life, non-toxicity and higher durability are the major factors that is driving the growth of this industry. The development of the Gallium Nitride and Indium Gallium Nitride based blue LED by Isamu Akasaki, Hiroshi Amano and Shuji Nakamura [1] was a giant leap in the field of LED lighting technology and has opened many new avenues for solid state lighting technology.

This blue light obtained at 450nm wavelength can be utilized in a wide array of applications by converting it into white light with the help of Yttrium Aluminium Garnet (YAG) phosphor by the process of Stoke's shift or by using Fluorescent SiC (f-SiC) co-doped with donor and acceptor pairs [2]. The various applications are indoor and outdoor lighting, LED backlight for TV screens or monitors, Automotive lighting. As the LEDs continue to operate for a long time and especially in high power applications, the joule heating effect comes into play and this rises the temperature of the LEDs by a significant amount.

This rise in temperature has some impact on the operating LEDs and leads to a decrease in their high temperature performance. In this paper, we will observe the impact that high temperatures have on the LED's output and find out the cause that is leading to the drop in performance that is a drop in the Light Output Power (LOP) which is also known as the Thermal droop or T-droop. The temperature of fixtures exceeds 85^{o}C which pushes junction temperatures over 120^{o}C, we find a reduction of

LOP by 20% compared to room temperature operation along with reduction in operational lifetime [3].

We will be considering some factors that can govern this phenomenon which are Shockley-Read-Hall recombination, Auger Recombination, Electron leakage, Piezoelectric Polarization and the Quantum Confined Stark Effect (QCSE) [4] and how it impacts the electron and hole wave-function overlap.

The contribution of each of the afore-mentioned factors will be studied and methods to overcome the negative impacts of these factors will be discussed. Once that is done an improved and advanced design of an LED stack will be proposed which should be able to have a higher quantum efficiency and be more efficient than the present-day LED technology at higher operating temperatures.

1.2 The Classic Double Heterostructure Light Emitting Active Region

The Light emitting diode is basically a forward biased P-N junction diode. The electrons are injected from the N side and the holes from the P side of the diode towards the active region. It is this active region of a Light Emitting Diode that involves most of the intricate and interesting device physics that all starts by the Double Heterostructure design.

To facilitate the recombination of Electrons and hole that were injected into the diode to release the energy in the visible spectrum we need to confine the careers. This need to confine the careers lead to the development of using different materials with a difference in Band Gap energy grown on top of each other of certain thickness. The Double Heterostructure design was thus born which would define the active region of LEDs in the form of Quantum Wells.

This Double Heterostructure active region helps in formation of quasielectric potential barriers that confine the electrons and hole and prevent them from flowing outside without blocking the flow of majority carriers [5]. The diagram below shows the Concept of Double Heterostructure used to confine electrons and holes for improved Radiative recombination.

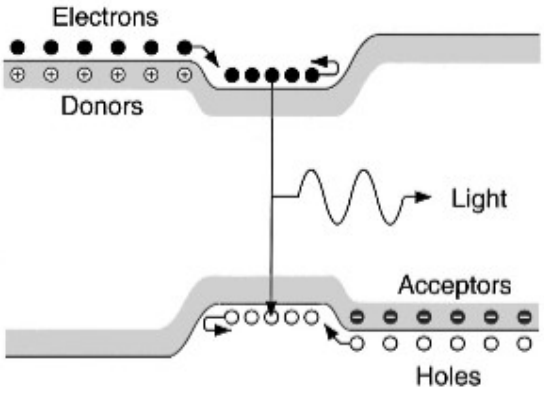

Figure 1.1: Double Heterostructure to confine Electrons and Holes for Radiative Recombination [5]

1.3 Hot/Cold Factor

This is a factor that we take into consideration while dealing with LED performance when the temperature is varying. Taking the LOP attainable from an LED at room temperature as the reference point, we compare the LOP of the same LED at different temperatures with it.

This procedure helps us identify the effect of temperature increase on the LED performance. We can compare the LOP of the device at a certain temperature with that of room temperature operation to get an idea and a picture of the device and how the performance degrades with increased LED junction temperatures.

This helps in simplifying the observation of T-droop in LEDs. The equation simply uses the quantum efficiency of the LED at different operating temperatures and is divided by the value at room temperature to find the percentage drop in performance.

It is represented as hot/cold factor

$$EQE(J)_{100^{\circ}C} \Big/ EQE(J)_{20^{\circ}C} \tag{1.1}$$

The percentage in thermal droop (%) [6]

$$(EQE(J)_{20^{\circ}C} - EQE(J)_{100^{\circ}C}) \Big/ EQE(J)_{20^{\circ}C} * 100\% \tag{1.2}$$

1.4 Carrier Recombination Mechanism Model

We will be referring to this carrier recombination mechanism model as we study about the various factors in this paper. The recombination mechanism in InGaN/GaN based Light Emitting Diodes is represented by equation 1.3 [7]:

$$R = An + Bn^2 + Cn^3 + f(n) \tag{1.3}$$

Here "A" stands for the Shockley-Reed-Hall recombination coefficient, "B" for the Radiative Recombination coefficient, "C" for the Auger Recombination coefficient and "f(n)" represents the leakage of carriers out of the active region which can even have higher than third order contributions to the recombination.

It has been found that the summed-up contribution of both Auger and f(n) leakage mechanisms comes out to be around $8*10^{-29} cm^6 s^{-1}$. It is also important to include the leakage term f(n) when dealing with InGaN/GaN LEDs because the theoretical ABC+f(n) data matches well with experimental results.

1.5 The Effect of Shockley-Read-Hall Recombination on Thermal Droop

SRH recombination is basically a trap assisted recombination which is caused by the traps present between the conduction band and valance band. It is based on the quality of material where the number of traps can be reduced by growing higher quality epitaxial layers which is a big thrust in shifting from growing epitaxial layers of GaN on sapphire substrate to GaN substrate. This removes the problem of high lattice mismatch of 16% [8] which can lead to dislocation defects increasing SRH recombination.

To understand the impact of SRH recombination on thermal performance some work was carried out by varying the temperature from 300K to 450K and at different current levels from 10mA to 2A.

We know from the recombination model the SRH recombination is proportional to the carrier concentration (n) and so we can say that the effect SRH recombination will have on the LOP of the LED will be higher at lower current levels and its contribution will decrease as the current levels keep increasing.

The LOP dropped 57.3% of its room temperature value at 450K at 10mA and it reduces as the current levels are increased. It was found that the SRH contribution was large at 10% of the total recombination at room temperature at 10mA which increased to 47.3% at 450K. The contribution was only 0.6% at 2A at room temperature and 3.1% at 450K [9].

The figure below shows the effect of Thermal droop on the External Quantum Efficiency of the experiment that was conducted. We can find the degradation in performance with every step rise in temperature.

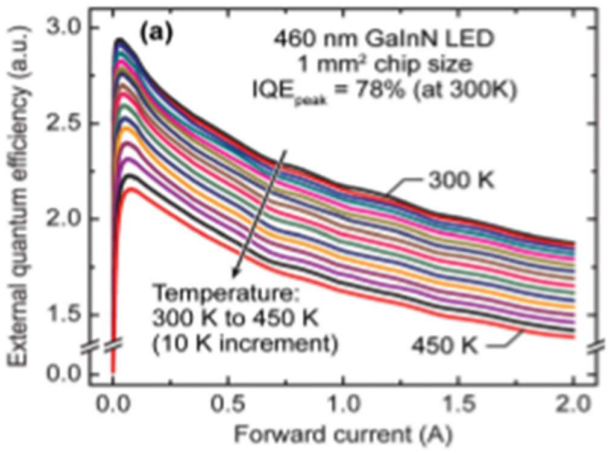

Figure 1.2: The Effect of Thermal Droop on External Quantum Efficiency of LED [9]

The next diagram gives an idea of the drop in Normalized LOP with temperature.

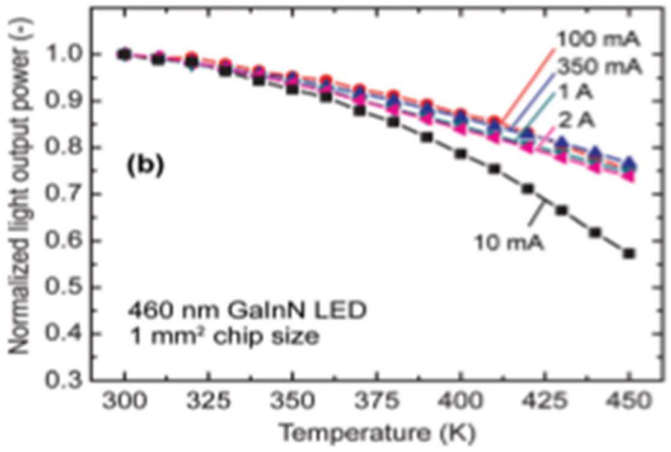

Figure 1.3: Normalized LOP for Different Temperatures [9]

The diagram here shows the contribution of SRH recombination as a factor in thermal droop. It can be seen from the diagram that since SRH is proportional to the lower orders of carrier concentration its effect is much more dominant when the current injection is less.

We will see later how carrier overflow comes into effect as we increase current injection and the effect of lower performance shift from SRH to other factors. We also find the experimental data of the SRH non-radiative lifetime to match closely to the theoretical fitting line. The decrease in lifetime indicates more non-radiative recombination thus leading to decreased quantum efficiency and LOP.

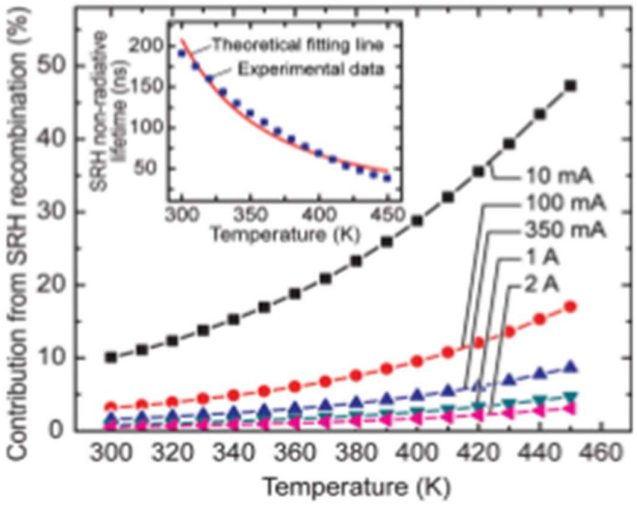

Figure 1.4: Percentage Contribution of SRH recombination and Non-Radiative SRH lifetime with temperature [9]

1.6 Chip Area and the Effect of SRH Recombination

We are all familiar by a phenomenon in LEDs called the Current droop or J-Droop which increases with the increase in current density. Manufacturers are slowly following a trend of increasing the chip area so that the current density is not very high when the LED is being used for high power applications. This will have a positive impact if we are only thinking about J-Droop. The bigger picture also contains the T-Droop which we know from above that is generally dominated by SRH recombination at lower current densities. The SRH Recombination Rate in an undoped quantum well is given by equation 1.4.

$$R_{SRH} = \frac{\delta(n)}{\tau_{nr}} = \frac{\delta(n)}{t_0} * \left(1 + \cosh\left(\frac{(E_t - E_{fi})}{KT}\right)\right) \quad (1.4)$$

where δ(n) is the concentration of excess electrons, τ_{nr} the non-radiative recombination lifetime, E_t and E_{fi} being the trap and intrinsic Fermi energies respectively while to is based on the capture cross section and trap concentration [10]. The following figures give us an idea of the trend that follows when we plot Normalized LOP against increasing temperature.

Figure 1.5 shows how the normalized LOP changes as the chip size changes which was calculated using three different chip areas with diameters of 200µm, 300µm, 500µm. Figure 1.6 shows the normalized LOP at various current densities for increasing temperatures which further strengthens our point of the dominance of SRH Recombination on the T-Droop at low current.

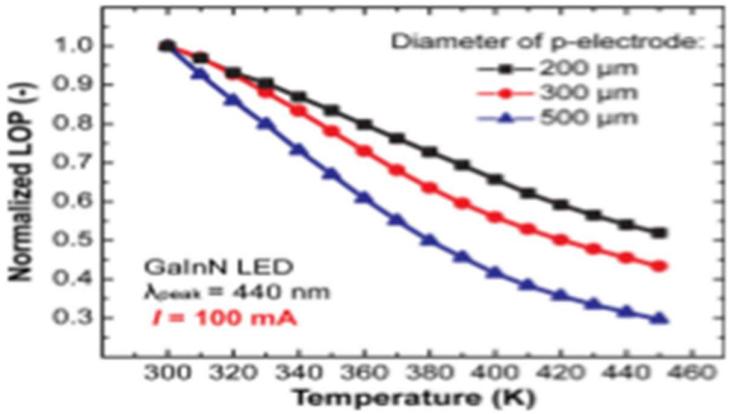

Figure 1.5: Normalized LOP for 3 Different Chip Areas [10]

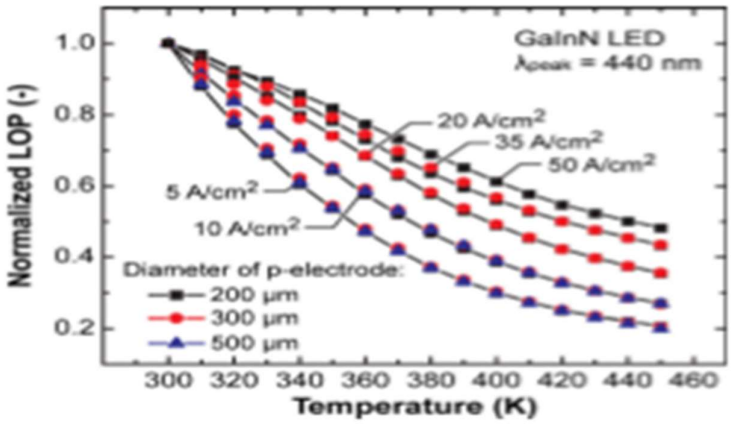

Figure 1.6: Normalized LOP for Different Current Densities [10]

The next chapter will deal with various factors that were directly involved in simulation, investigation and analysis of the thermal performance of LED device.

2.1 Carrier Leakage out of the Active Region

This a very important factor that needs to be taken into consideration when we are talking about the LOP of LEDs with varying operating temperature or operating current levels. Now we know the total recombination ABC model and we make a slight change to it because of the ambiguity of C and other third order terms, we include all that in the term f(n). The contribution of f(n) to the total recombination can be expressed by equation 2.1

$$Y = \frac{f(n)}{(An+B\ ^2+Cn^3+f(n))} \tag{2.1}$$

Studies show that the contribution of f(n) is 12.7% of the total recombination at a current level of 10mA but a contribution of 49.3% at 2A. Also, we find that at a current level of 350mA the f(n) contributes 30.5% at room temperature while at 450K it contributes 39.3% [9].

Thus, we see that with the increase in temperature it becomes more difficult to contain the carriers specially electrons which are at a higher energy that is leading to them overflowing out. We also see that at a current level of 350 mA the IQE drops from 67.8% at room temperature to 52% at 450K the measured drop in LOP comes out to be 23.4% with the increase in SRH recombination contributing to 10.4% and the increase in f(n) term contributing to 13% [9].

In the figure below we can see the contribution of f(n) to the total recombination at different temperatures and different current levels. We also see that in case of the lower current levels like 10mA the contribution of the f(n) term decreases at higher temperatures because we know from above that SRH recombination dominates at lower

current levels and even though the value of f(n) has increased with increase in temperature, it was dominated by an even higher increase of SRH recombination thus we see a decrease with increase in temperature.

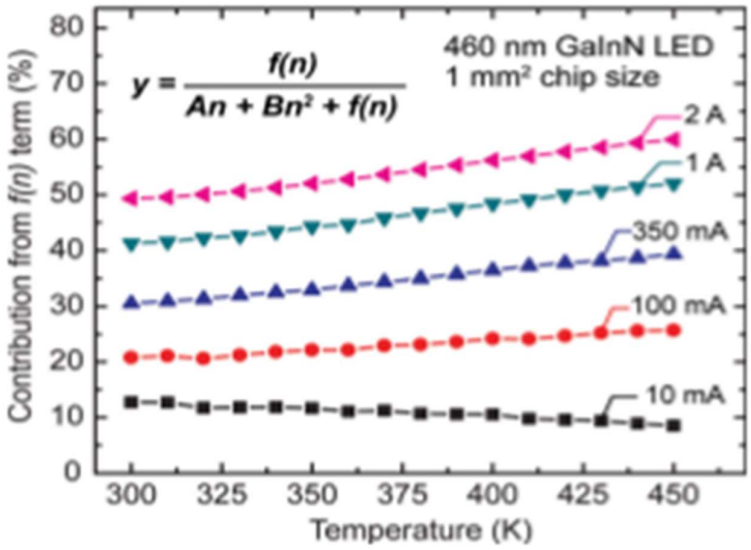

Figure 2.1: Percentage Contribution of Electron Leakage f(n) to Total Recombination [9]

2.2 Piezoelectric Polarization Effects

The Ga-N bond has a polar nature and the lack of inversion symmetry in a Wurtzite crystal, III-Nitrides have spontaneous and piezoelectric polarization [4]. Spontaneous polarization is an intrinsic property related to the nature of the bonds and is present in the lattice in equilibrium. Piezoelectric polarization is present in psuedomorphically grown strained layers.

The total polarization is the sum of the two. Sheet charges are induced at the layer interface of the adjacent layers because of discontinuities in the normal components of the total polarization. It is represented by the formula 2.2

$$\left(P_{sp} + P_{pz}\right)_{lay} - \left(P_{sp} + P_{pz}\right)_{layer2} = \sigma_{pol} \qquad (2.2)$$

Where P_{sp} and P_{pz} are spontaneous and piezoelectric polarizations and σ_{pol} is the induced sheet charge. The total polarization discontinuity in the growth direction depends on the crystal orientation. Figure 2.2 below shows us how it varies by changing the inclination angle from the polar c-plane in a coherently strained $In_{0.2}Ga_{0.8}N$ layer on GaN [11].

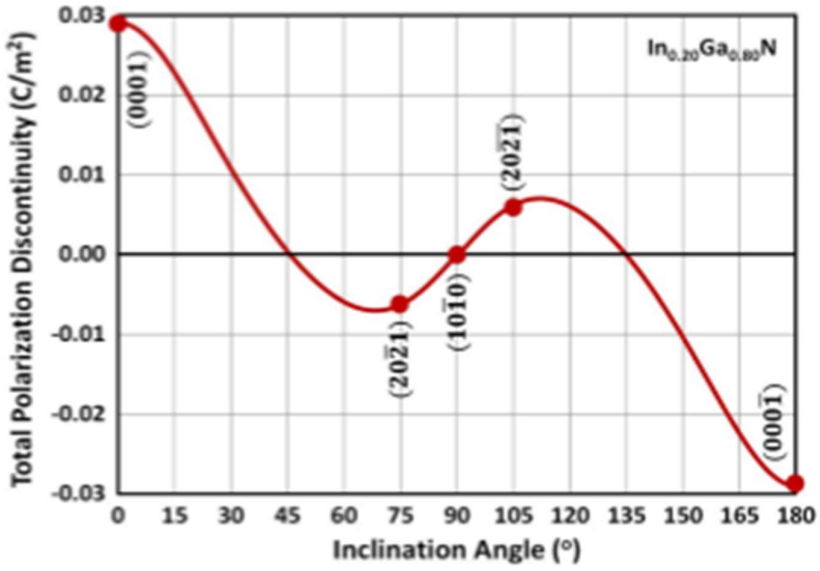

Figure 2.2: Total Polarization Discontinuity vs. Inclination Angle [11]

From this figure, we see that certain orientations can help reduce or even remove the total polarization discontinuity like the non-polar plane $(10\bar{1}0)$. The max polarization discontinuity is present in the polar c-plane (0001). The interface sheet charges induce polarization related electric fields which exist along with the p-n junction built in fields. In a Single Quantum Well (SQW) the electric field due to polarization is given by:

$$E_{qw} = E_{spqw} + E_{pzqw} = \frac{(P_{sp}b - P_{spqw})}{e_{0qw}} - P_{pzqw}/e_{0qw} \quad (2.3)$$

where P_{spb} and P_{spqw} are the spontaneous polarization in barrier and quantum well and e_{0qw} is the dielectric constant in the quantum well [12].

The polarization related electric field influences the bandgap of the material. In the polar c-plane (0001) we see that the E_{pz} is anti-parallel to the built-in field E_{bi} and is much stronger so this makes the bands slope in an opposite direction to the p-n junction slope.

In the semi-polar $(20\bar{2}1)$ plane the two fields are parallel to each other and they add up giving rise to a slightly steeper slope in the same direction as that of the p-n junction slope. In $(20\bar{2}\bar{1})$ the fields have similar magnitude and are opposite to each other thus cancelling each other out resulting in an almost flat band structure. The non-polar m plane has 0 polarization field so the bands are sloped based on only the E_{bi} field.

This variation of band slope brings us to the electron and hole wave-function overlap. The more the slope of the bands, less the wave-functions will overlap as the electrons and holes will be forced to go to the opposite ends of the quantum well thus reducing the radiative recombination rate.

It has also been observed that with the increase in "In" composition, there is an increase in the piezoelectric polarization. The slopes on c-plane and semi-polar $(20\bar{2}1)$ will increase but at 25% In composition the bands will be flat for semi-polar $(20\bar{2}\bar{1})$ and the non-polar m-plane will be unaffected.

Figure 2.3 below will give a better understanding of the effect total polarization has on the electron-hole wavefunction [12]. This helps to us to understand the

wavefunction overlap and gives us an idea of the probability of effective radiative recombination which is the basis of internal quantum efficiency of an LED device.

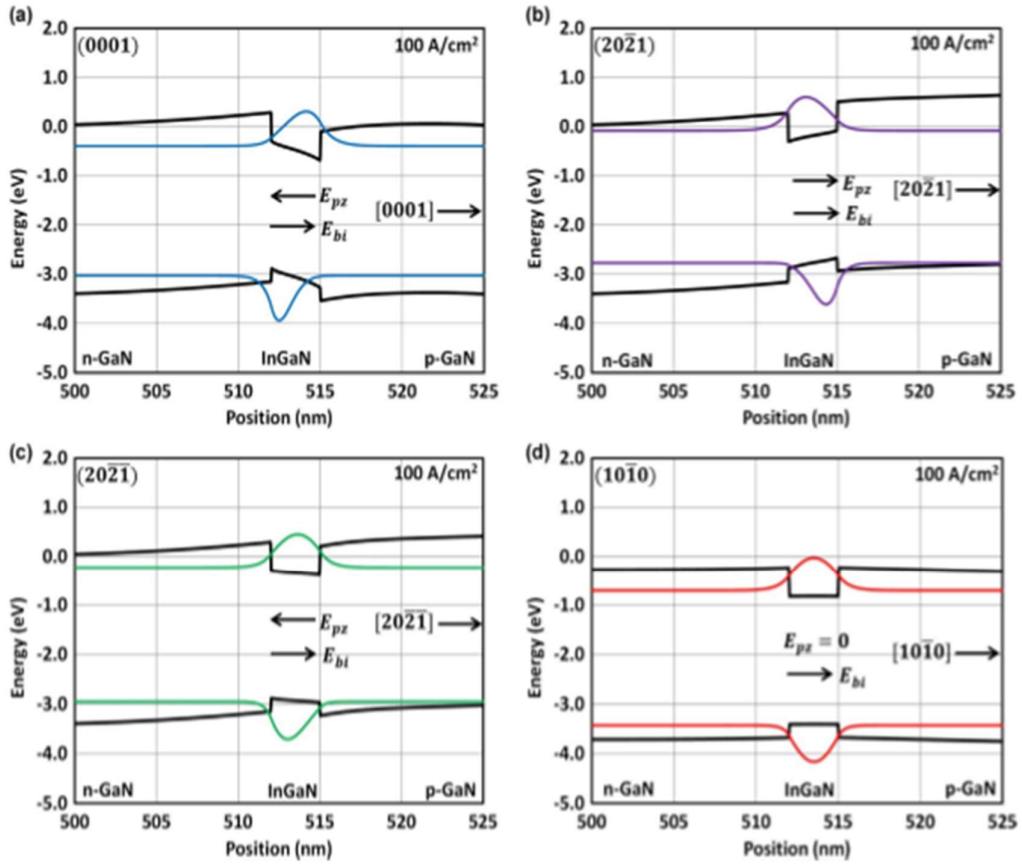

Figure 2.3: Band Structure and Wavefunction of the Four Different Planes [12]

2.3 Using Electron Blocking Layers

Electron blocking is an important factor that should be taken into consideration when we are dealing with LEDs. With the help of proper electron blocking we can prevent the electrons from overflowing or escaping out of the active region. The term f(n) which we encountered earlier is the main reason why we use an electron blocking mechanism.

A study was conducted to see how an electron blocking layer (EBL) of varying thickness can be used to improve thermal performance of LED. Four LEDs were taken out of which three had EBLs with thickness of 20nm, 40nm and 60nm made of AlGaN [13].

The LEDs were put to the test and it was found out that the one with 20nm EBL showed the best performance and the one without any EBL had the worst performance.

The reason why the other EBL LEDs could not outperform the 20nm one was that due to the valance band offset between GaN/AlGaN there was a barrier created for holes to be able to come into the active region which was exacerbated with increase in thickness [12].

From figure 2.4 below we can see that if the temperature increases a lot, the performance of the 20nm EBL drops a lot compared to the other LEDs with thicker EBLs thus suggesting the reduction of effective electron blocking at higher temperatures by a thinner EBL.

This problem can be overcome by using a GaN buffer layer between the wells and the EBL. Thus, helping to keep the overall valance band offset low as well as help prevent the overflow of electrons at higher temperatures as we will see later.

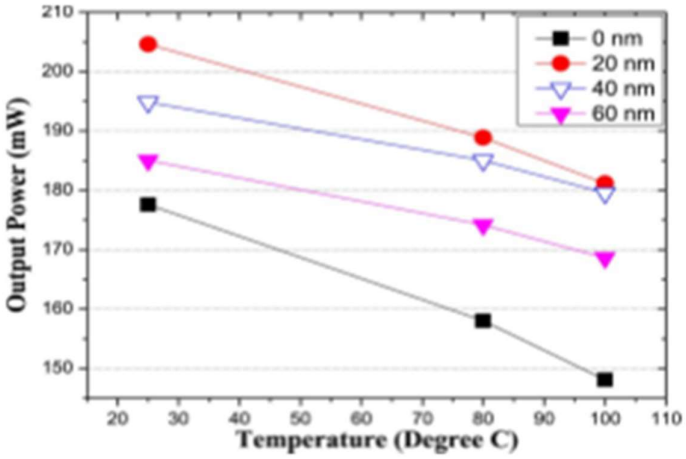

Figure 2.4: Output Power vs. Temperature for EBLs of Different Thickness [13]

Electron blocking mechanism thus shows us that it can be effective in improving the thermal performance of LEDs. EBLs have certain problems like a lattice mismatch causes a degree of piezoelectric polarization which tends to pull down the conduction band offset thus reducing its effectiveness.

An improved design of using an Electron Blocking Super Lattice structure can be used with graded Al concentration [14]or an AlInN based Super Lattice having a better lattice match with GaN [15] [16] [17] can be developed having lower piezoelectric polarization and less valence band offset as well.

For simplicity of design to keep it effective and easy to grow our device EBL structure will have a thinned out AlGaN EBL to reduce overall Aluminium content thus keeping the piezoelectric fields less along with a thin GaN buffer layer for effective electron blocking and improved hole transport.

2.4 Reducing the Number of Quantum Wells

This is an important factor that needs to be considered while making an InGaN/GaN LED device. It is imperative to understand the number of quantum wells

that will be needed for optimized LED radiative performance. One of the works by Nakamura [18] showed that the lowest current density threshold could be obtained for two wells when the number of quantum wells were varied from single to four wells.

Another work [19] found out that the lowest value of threshold current density could be obtained in a single well Laser Diode design with wavelength of emission equal or longer than 435 nm. The reason being the high InGaN dissociation pressure that caused high Indium content well layers to dissociate at high growth temperatures of 750 ^{o}C [20].

LASTIP simulation software was used by Chang et al, 2002 [21], Chang et al, 2003 [22], Kuo et al, 2004 [23] to study the performance of laser diodes which reduced with increase of number of quantum wells. One of the factors was hole inhomogeneity within the wells.

SILVACO/ATLAS simulation tool was used to compare the performance of $In_{0.13}Ga_{0.87}N$ quantum wells single vs. multi quantum well design [24]. The simulation results showed a decrease in the radiative recombination rate with increase in number of wells used. Figure 2.5 below shows the integrated radiative recombination rate with respect to the number of quantum wells used in the device.

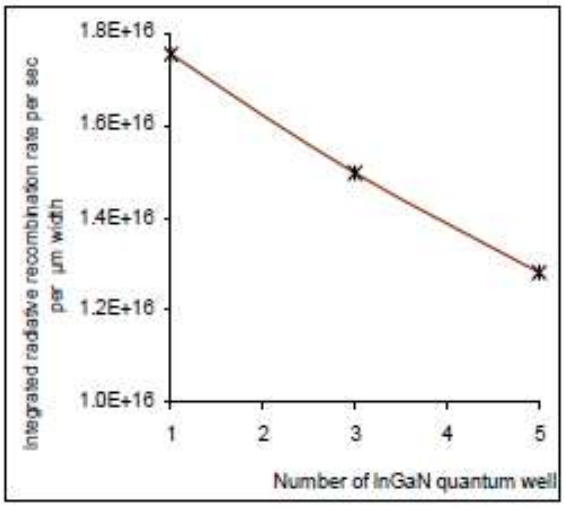

Figure 2.5: Integrated Recombination Rate vs. Number of Quantum Wells [24]

The 5-QW design had inhomogeneous distribution of electrons throughout the different wells. The hole concentration was a bit more homogeneous. The higher valance band offset and lower mobility of holes inhibited their transfer to the wells towards the "N" doped side. This resulted in the last three quantum wells to be unproductive thus reducing the overall efficacy of the device.

With this knowledge, the initial step was to develop a thick single quantum well design for an improved LED design for high thermal performance but certain factors needed to be considered thus moving on towards a different design.

2.5 Shifting away from using a Thick Single Quantum Well design

The previous section talks about reducing the number of quantum wells used in the device for efficient LED operation. Thus, removing all the wells and using a single quantum well might seem as a good option but certain other factors need to be considered. A Thick single quantum well design has some advantages which lead to improved LED performance.

The advantages are due to a larger volume, the total effective volume for the careers increase which tends to inhibit the effect of Auger Recombination at high current injections thus improving Internal Quantum Efficiency.

This problem is tackled well when using a 12nm Thick Single Quantum Well structure grown on semi-polar $(20\bar{2}\bar{1})$ plane with low piezoelectric polarization. This lead to Thermal droop of only 9.7% from 20^{o}C to 100^{o}C whereas the droop was over 20% for the C-plane grown Single Quantum Well [25].

To keep the device materials relatively easily available and to simulate GaN on SILVACO, the simulations were done using the C-plane that suffers from relatively high piezoelectric polarization. This relatively high piezoelectric effect will not allow proper functioning of the Thick Single Quantum well design as it will increase the spatial separation of electrons and holes, exacerbating the Quantum Confined Stark Effect even further [26].

Figure 2.6 [26] below shows how a Thick Quantum Well when grown on a high piezoelectric plane suffers from increased spatial separation of electrons and holes, decreasing their effective volume, reducing the overlap area of their wavefunctions which ultimately leads to decreased radiative recombination.

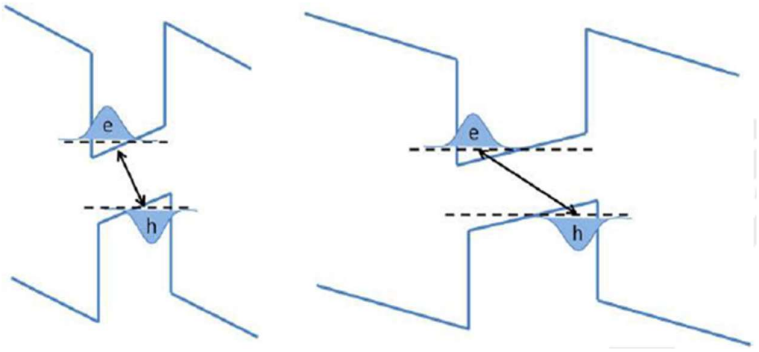

Figure 2.6: Comparing the Electron-Hole Recombination for QWs of Different Thickness [26]

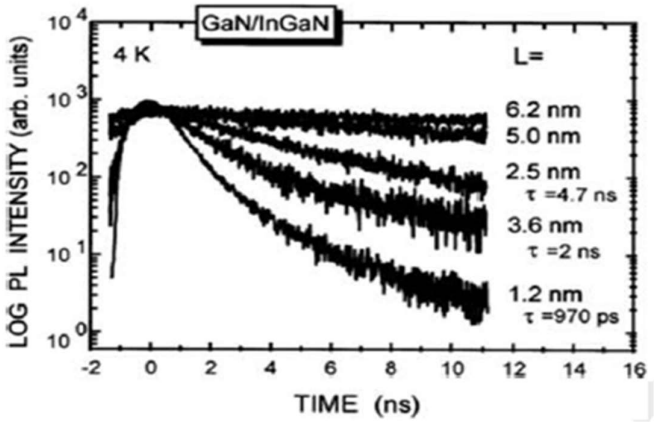

Figure 2.7: Time Resolved Decay Curves for Different Well Thickness [26]

Figure 2.7 shows us the PL intensity of the time resolved decay curves for quantum wells of different thickness. It is observed that the wells of less thickness have the shortest decay times compared to wider wells. This is important to increase the amount of radiative recombination taking place in the active region wells of the LED device.

In the next chapter, we will develop the LED device structure based on the concepts we have encountered till now and simulate three slight variations keeping the overall structure the same. This will help us understand how the different designs work under high temperature conditions.

THE DEVICE FOR IMPROVED THERMAL PERFORMANCE

3.1 The Device Structure

Figure 3.1 represents the schematic of the dual well structure LED design with a thin Electron Blocking Layer that has been specifically designed to improve performance at high temperature operating conditions by suppressing some factors that contribute to Thermal droop.

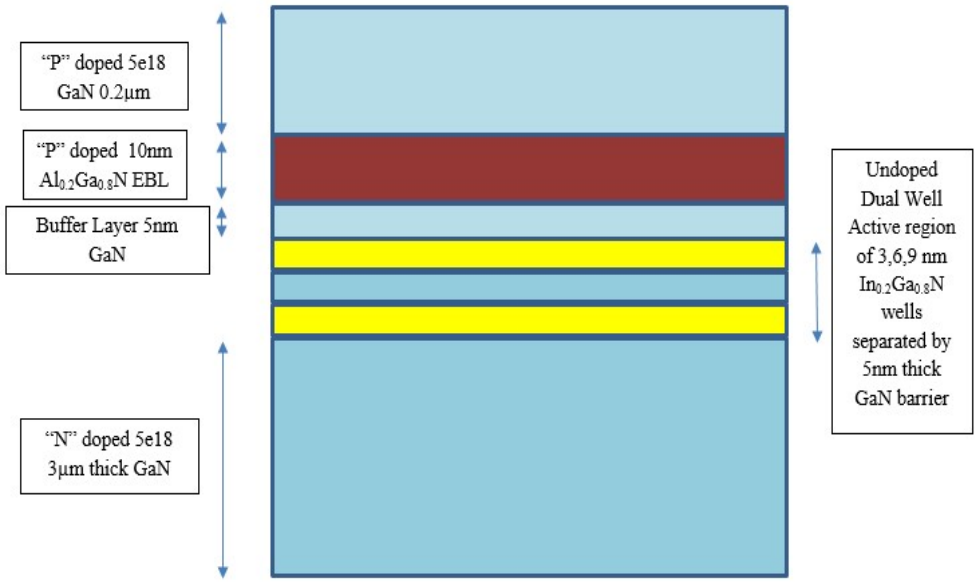

Figure 3.1: Schematic Diagram of the Dual Well Structure

This device structure used has a simple yet effective design which focuses a great deal on problems such as electron leakage "f(n)" from quantum wells, hole transport. This issue can be addressed and improved upon using the Dual Well design where an extra well is used as an assisting well that assists the operating well when the system is forced into high temperature operation.

This technique is effective in not just reducing the effect of thermal droop but slightly improving the Internal Quantum Efficiency as we move from 300K to 400K

operating temperatures. Three different well dimensions of 3nm, 6nm and 9nm were simulated using SILVACO/ATLAS to analyse operation of the wells.

3.2 SILVACO TCAD Models

3.2.1 Polarization Model

Including the Polarization model is imperative when dealing with Gallium Nitride based devices because of the inherent piezoelectric polarization charges due to the Wurtzite structure. To introduce this model into the TCAD deck we need to specify POLARIZATION in the region or material. This helps to include the effects of spontaneous and piezoelectric polarization as seen in equations 3.1 and 3.2 [30] in the regions we need these calculations such as at an interface of the heterostructure or the active region quantum wells.

Total Polarization:

$$P_t = PSP + P_{pi} \tag{3.1}$$

Where PSP is specified in the material statement as total spontaneous polarization.

Piezoelectric Polarization:

$$P_{pi} = 2\frac{a_s - a_0}{a_0}\left(E_{31} - \frac{C_{13}}{C_{33}}E_{33}\right) \tag{3.2}$$

Here E_{31} and E_{33} are the piezoelectric constants, C_{13} and C_{33} are the elastic constants. The lattice constant of the material layer is a_0 while as is the average value of the layers above and below it. This model is simulated by adding positive and negative fixed charges that are added to the top and bottom of the layer that is being considered.

3.2.2 Incorporating Strain and Scaling the Polarization Charge

Since we are incorporating AlGaN and InGaN into our device structure, we will be changing the lattice structure slightly which will bring in the factor of strain. It is important to incorporate this strain into our simulation to accurately simulate and analyse the behaviour of electrons and holes. Specifying calc. strain [27] in the simulation makes the simulator calculate the strain caused from the lattice mismatch of the layers used.

It is important to scale the polarization charges because the default scale value is 1.0 which can be a bit too strong for the simulator to converge the calculations. Since we are using only 20% of "Al" or "In" in our layers and using relatively thin layers like a 10nm thick AlGaN EBL and thin quantum wells of 3nm, 6nm we keep the scale to 15% of the default value. This scaling can be done using *polar.scale* model [27].

3.2.3 Using the K.P Model

Since we are using quantum wells which have different composition from the bulk material, we need to take in to account the variation in band structure and the effective masses of the careers. Thus, we need this k.p model for semi-empirical method of calculating the band structures, the effective masses and the optical properties of the crystal [28].

This model is also effective to find the analytic expression for band dispersion, zone from zone centre energy gaps and the matrix of optical elements [29].

3.2.4 Involving Shockley-Read-Hall Recombination

Traps or defects within the energy band gap of semiconductors can cause phonon transitions. It is a material parameter and these traps capture the electrons and

holes, causing a degradation in the internal quantum efficiency. The Radiative recombination rate is given by equation 3.3 [27]

$$R_{SRH} = \frac{pn - n_{ie}^2}{\tau_P\left[n + n_{ie}exp\left(\frac{ETRAP}{kT_L}\right)\right] + \tau_n\left[p + n_{ie}exp\left(\frac{-ETRA}{kT_L}\right)\right]} \quad (3.3)$$

Here ETRAP stands for the difference in energy between the trap levels and the Intrinsic Fermi, TL is the lattice temperatures in Kelvin, τ_p and τ_n are the concentration dependant life times. To involve the SRH model into the simulation, we need to specify *consrh* in our model statement.

3.2.5 Auger Recombination

This phenomenon occurs through a three-particle transition. Here a mobile carrier is either captured or emitted. It is given by the equation (3.4) [30].

$$R_{AUGER} = AUGN(pn^2 - nn_{ie}^2) + AUGP(np^2 - pn_{ie}^2) \quad (3.4)$$

To incorporate this model into the simulation deck we need to write *auger* parameter in the models statement.

3.2.6 Optical Radiative Recombination

Since we are simulating an LED device it is important to involve the optical radiative recombination mechanism. This process happens in one step thus it's a direct recombination mechanism. The electron in the conduction band loses its energy and then comes down to the valance band. The energy released in our LED is in the blue region. We need to factor in the capture rate to C_c^{OPT}. The equation 3.5 [27] gives us an understanding of the mechanism.

$$R_{np}^{OPT} = C_C^{OPT}(np - n_{ie}^2) \quad (3.5)$$

C_c^{OPT} is defined by *copt* on the material statement and the optical recombination/generation model can be defined by *optr* in the models statement.

3.3 Energy Band structure of the device at unbiased condition

Figure 3.1 represents the schematic of the dual well structure LED design with a thin Electron Blocking Layer that has been specifically designed to improve performance at high temperature operating conditions by suppressing some factors that contribute to Thermal droop.

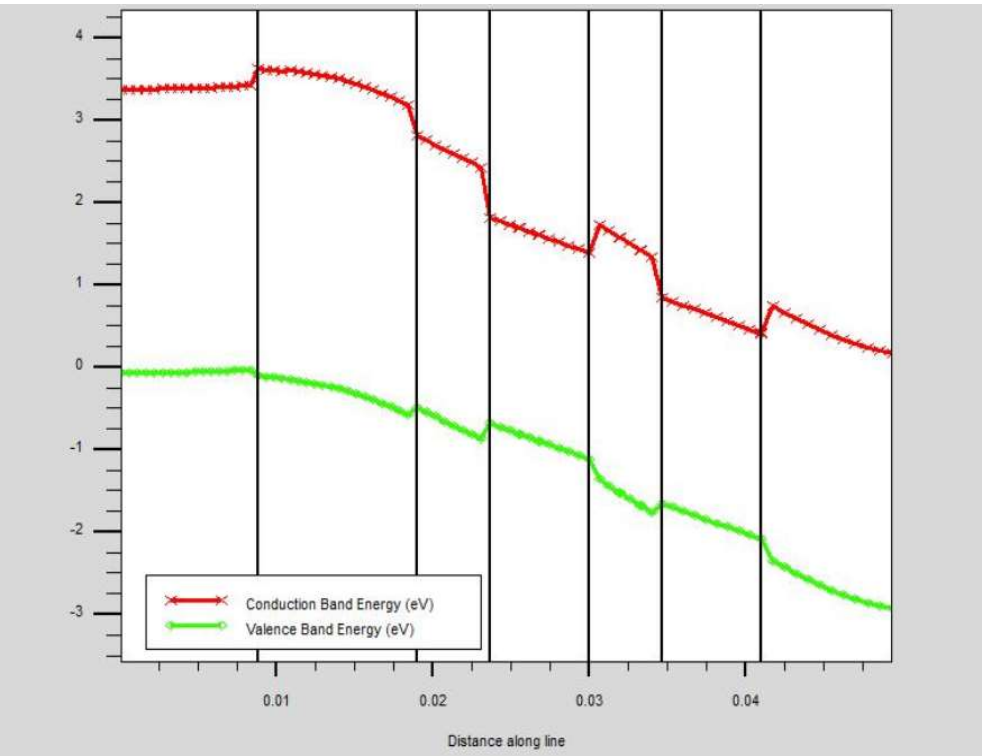

Figure 3.2: Energy Band Structure at 0V and 300K

Figure 3.1 represents the schematic of the dual well structure LED design with a thin Electron Blocking Layer that has been specifically designed to improve performance at high temperature operating conditions by suppressing some factors that contribute to Thermal droop.

In the simulation, the LED will be biased from 0V to 6V and various output parameters such as I-V curve, Electron and Hole bound density, Light Output Power, Power Spectral Density, Electron-Hole Wavefunction Overlap and Internal Quantum Efficiency data will be examined and analysed. These output graphs will be compared among 3nm, 6nm and 9nm wide wells which will give us an idea of the difference in their operations.

3.4 Optimizing the EBL based on Hole Transport

Two structures were taken with the same design of a bulk $Al_{0.2}Ga_{0.8}N$ EBL and a 5nm GaN buffer layer. A thick EBL structure will have a high overall Al content leading to increased lattice strain and stronger piezoelectric fields. This tends to pull down the EBL structure increasing the Valance band offset and decreasing the Conduction band offset.

The result ends up in reduced hole transport into the active region wells and weaker electron blocking. Figures 3.3 and 3.4 below will show the graph of Hole Bound Density for two device structures one with a 20nm thick EBL and another is a 10nm EBL at 300K.

Focusing on Well 1 we can see the hole bound density peak for the 20nm design is at $2.25e^{19}$ cm^{-3} and is a much thinner curve pushed to the edge of the well due to stronger piezoelectric fields and Well 2 also tops out at $4.5e^{19}$ cm^{-3}.

In the 10nm EBL design, the Well 1 peak hole bound density is at $3e^{19}$ cm^{-3} and is a much broader curve that covers the full width of the well. Well 2 hole bound density peaks at almost $6e^{19}$ cm^{-3}. The LED was simulated at an applied voltage of 3.5V at 300K.

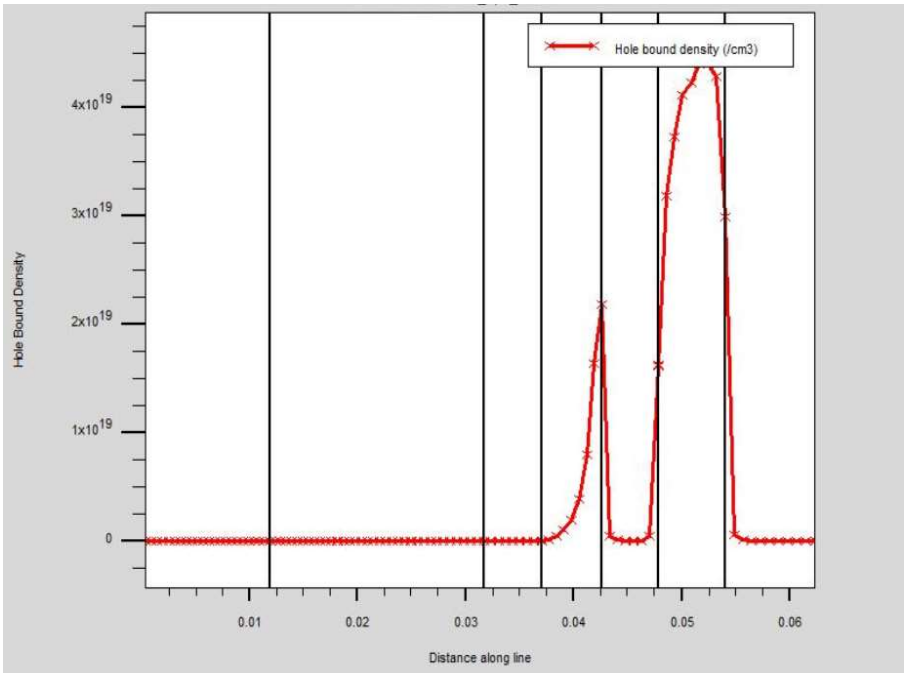

Figure 3.3: Hole Bound Density of 20nm Thick EBL Device at 300K

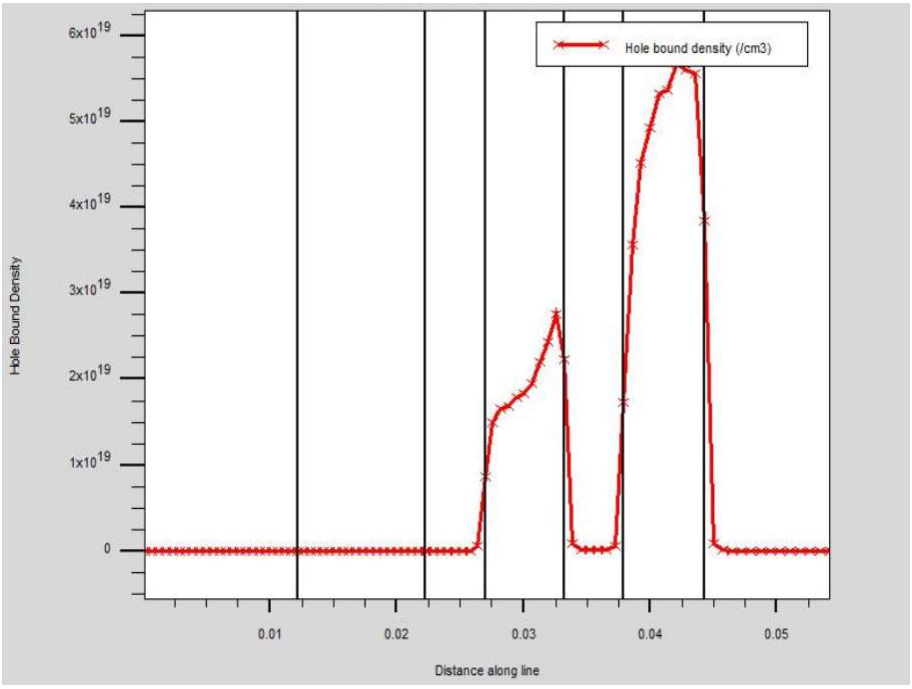

Figure 3.4: Hole Bound Density of 10nm Thick EBL Device at 300K

3.5 Variation of the I-V Curve with Temperature

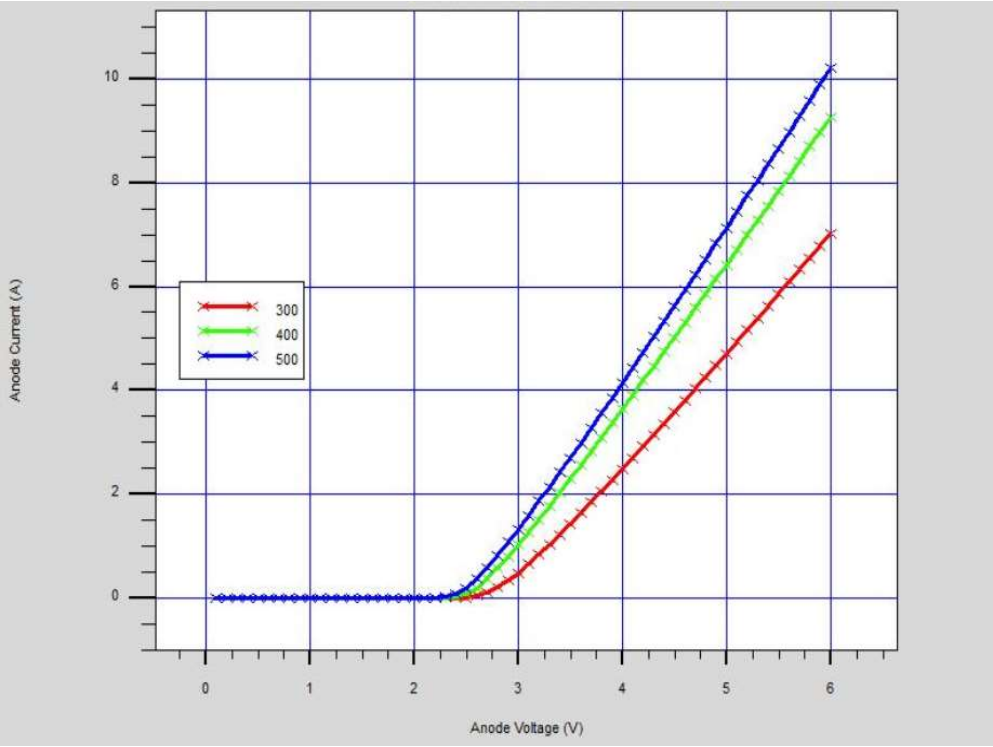

Figure 3.5: I-V Curve of LED Device at 300K, 400K and 500K

In Figure 3.5 we can see how the I-V curve of the device varies as the temperature is changed. The device voltage bias was changed from 0V to 6V and the current was recorded at 300K, 400K and 500K which are the three main temperatures we will be using to understand the behavioural trend of the device based on its output parameters.

We find that for a given voltage the current in the device increases as the temperature is increased. At higher temperatures, the value of the effective density of states increase which increases the value of the intrinsic carrier concentration and causing a drop in the built-in potential that ultimately leads to increase in the concentration of the carriers. This causes a boost in the device current for a given voltage when the temperature is increased.

RESULTS AND ANALYSIS OF THE DEVICE PERFORMANCE

4.1 Light Output Power

The Light Output Power (LOP) of the devices having 3nm, 6nm and 9nm wide wells were simulated. LOP is the rate of radiant flux emerging from the active region of the device per unit time. The simulations were carried out at 300k, 400K and 500K as we can see from the Figure 4.1, 4.2, 4.3.

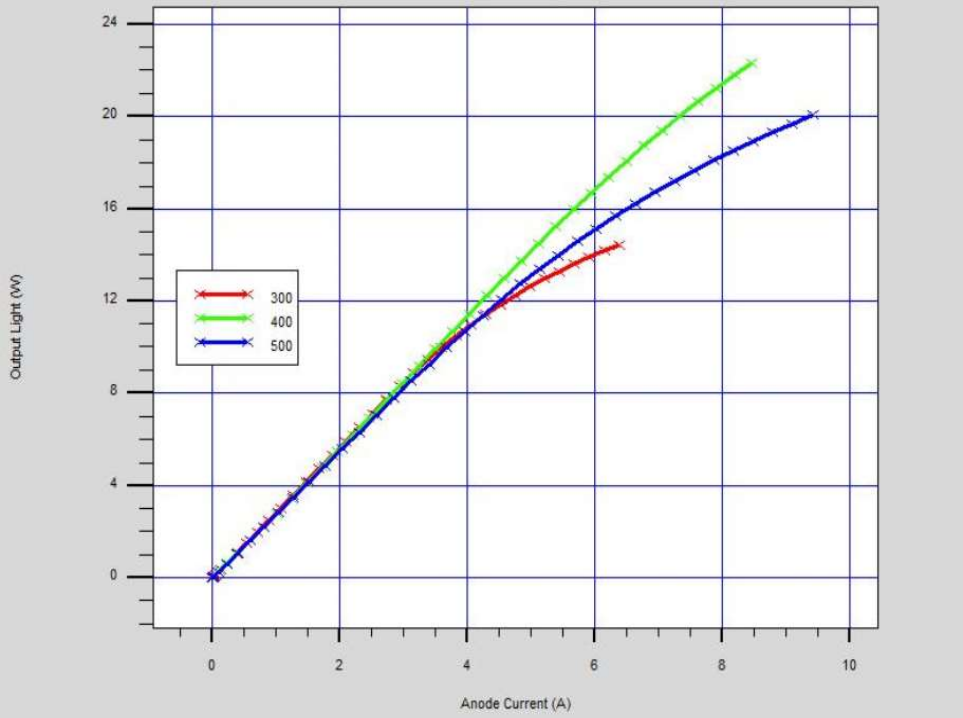

Figure 4.1: Light Output Power for 3nm Wide LED

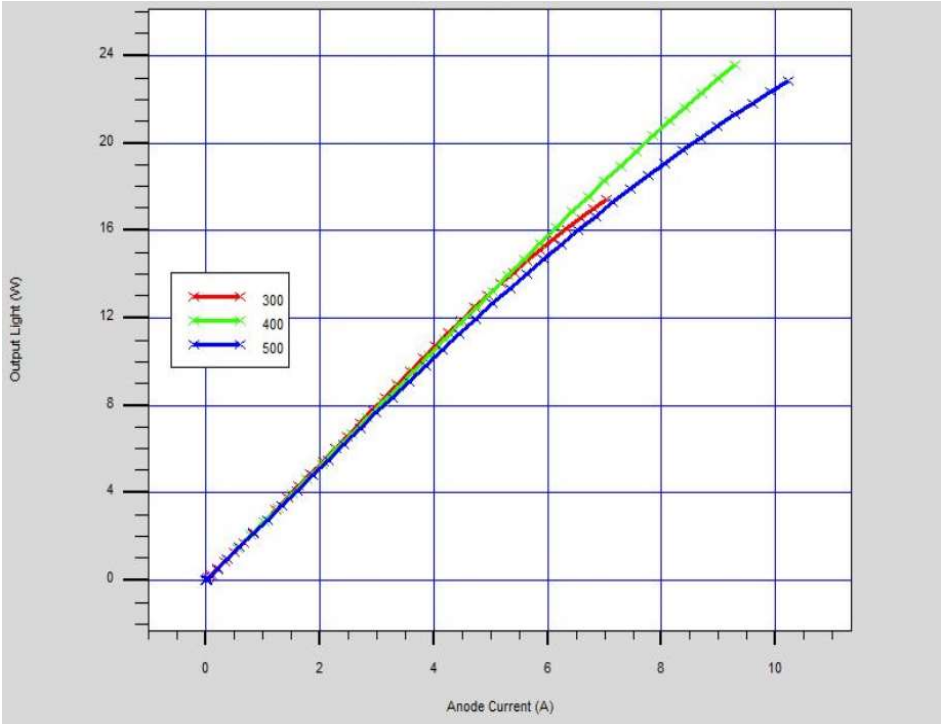

Figure 4.2: Light Output Power for 6nm Wide LED

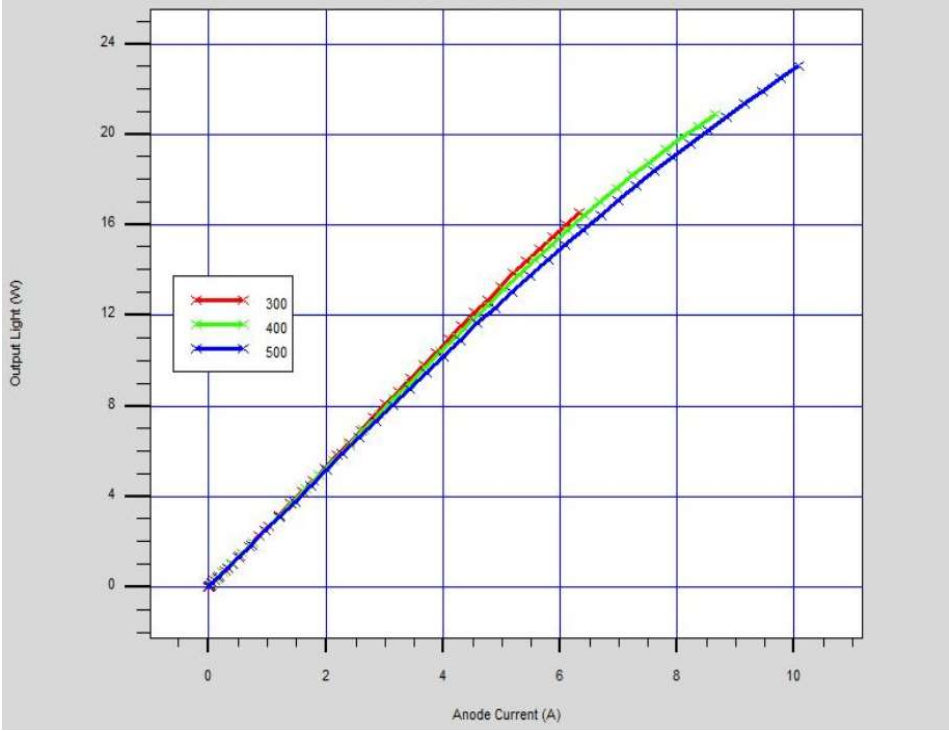

Figure 4.3: Light Output Power for 9nm Wide LED

From the figures above we can see the behavioural trend of the LOP for 3nm and 6nm wide LEDs are similar while that of the 9nm wide well is different. The trend which the first two LEDs follow has the LOP at 400K higher for a given current than that at 300K. Then at 500K the LOP of the LEDs drop down which we suspect decreased radiative recombination rate as understood by the graphs of Internal Quantum Efficiency later in this paper.

4.2 Variation of Internal Quantum Efficiency

In the figures 4.4, 4.5, 4.6 we will be able to observe the variation in Internal Quantum Efficiency curve and how the Thermal Droop varies when the three different devices are simulated. Internal Quantum Efficiency is basically the ratio of all the electrons that have been able to recombine radiatively and released its energy in the electromagnetic spectrum over all the electrons that recombined in the device. Thus, deriving from equation 1.3 we can get 4.1

$$IQE = \frac{Bn^2}{(An+Bn^2+Cn^3+f(n))} \tag{4.1}$$

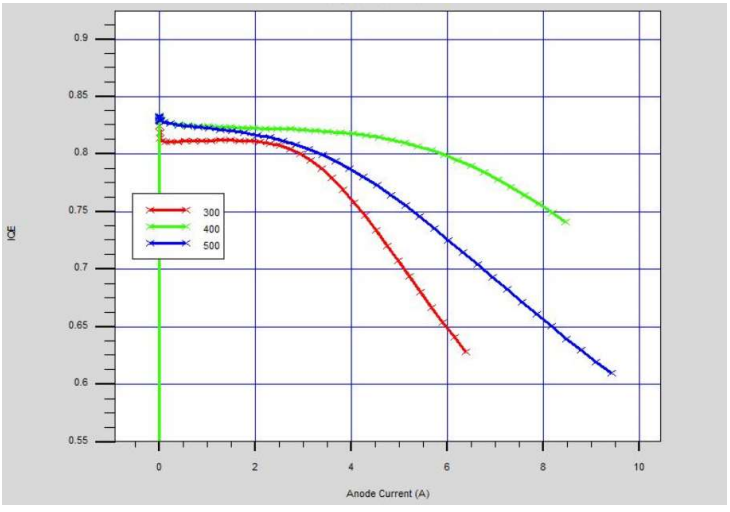

Figure 4.4: IQE of 3nm Wide LED for 300K, 400K, and 500K

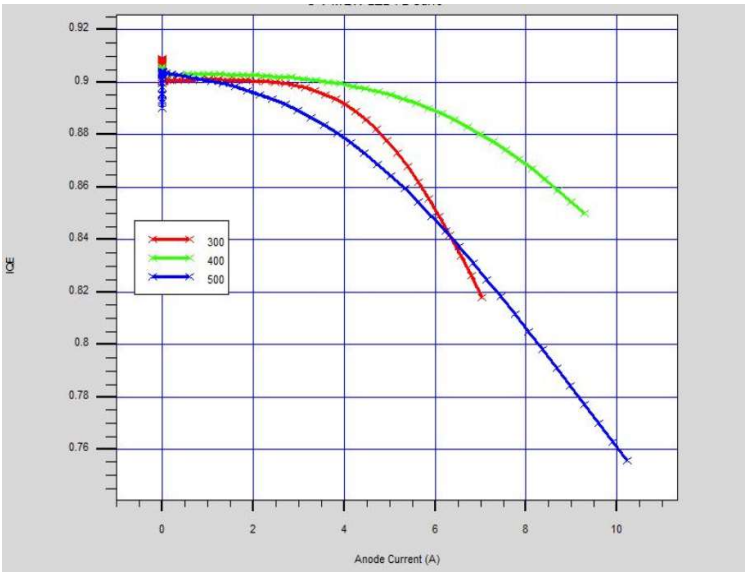

Figure 4.5: IQE of 6nm Wide LED for 300K, 400K, and 500K

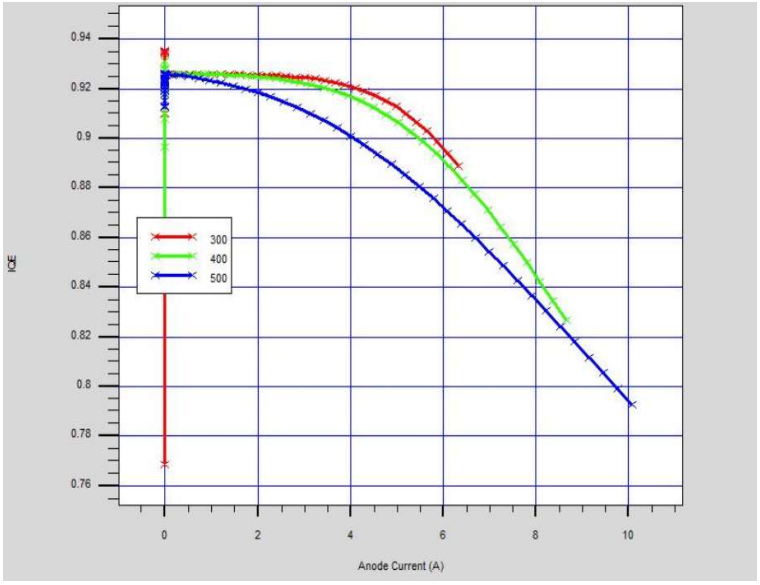

Figure 4.6: IQE of 9nm Wide LED for 300K, 400K, and 500K

In the above figures the three different LED devices have been simulated for 300K, 400K and 500K. The first thing we observe is the increase in the length of the curves as the temperature increases which is attributed to the increase in device current with temperature as explained in section 3.5.

Focusing on the trend we find the relation between the 300K and 400K IQE graphs for the 3nm and 6nm devices to be similar. The surprising feature that we encounter here is the improvement in the IQE as we go from 300K to 400K (a detailed IQE trend for 6nm device will be shown later in the paper from 300K to 550K with 25K interval).

Shifting our focus to the 9nm wide well device we find that the trend is normally as we would find in any existing LED device undergoing the thermal droop effect as the IQE curves fall vertically downwards with increase in temperature. The dual well structure plays an important role in making this phenomenon happen.

We will see later in the paper in details how the electron, hole bound density vary with temperature inside the wells that lead to a big change in the percentage overlap of the electron-hole wave functions and consequently leading to variations in the Power Spectral Density.

4.3 Variation in Power Spectral Density (PSD)

Power Spectral Density of a signal basically indicates the amount of power that is present in the signal as a function of frequency. This output parameter is important to understand the strength of the light that will emerge out of the wells based on frequency. Thus, we will be able to find out at what wavelength the LED light output is peaking and how the wells of the 3nm, 6nm, 9nm devices are radiating with variation in temperature. The figures below will give us an idea of the how the two wells behave at different temperatures which would indicate towards an explanation of the unusual trend of the IQE that we saw before.

4.3.1 Power Spectral Density Curves of 3nm Device (Red-Well 2, Green-Well 1)

In the figures from 4.7 to 4.15 we can observe the variation in the PSD of the 3nm wide dual well structure. Here we see at 300K, the peaks of the two wells don't align properly which we suspect due to the strong piezoelectric field that distort the wells and alter the bandgap. We see that at 300K both the wells are radiating.

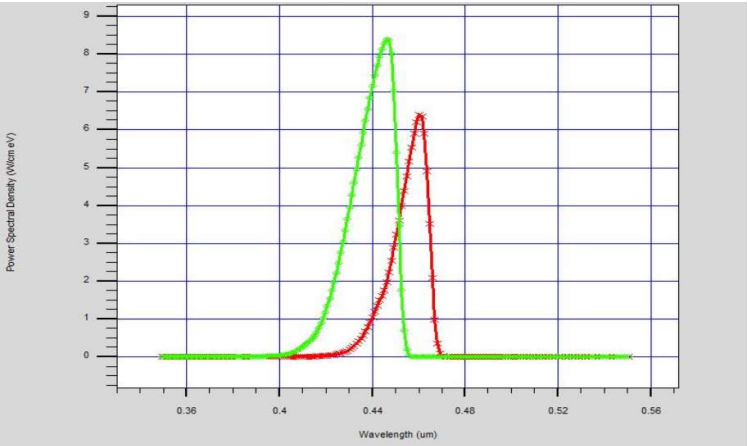

Figure 4.7: Power Spectral Density Curve for 3nm Device at 300K

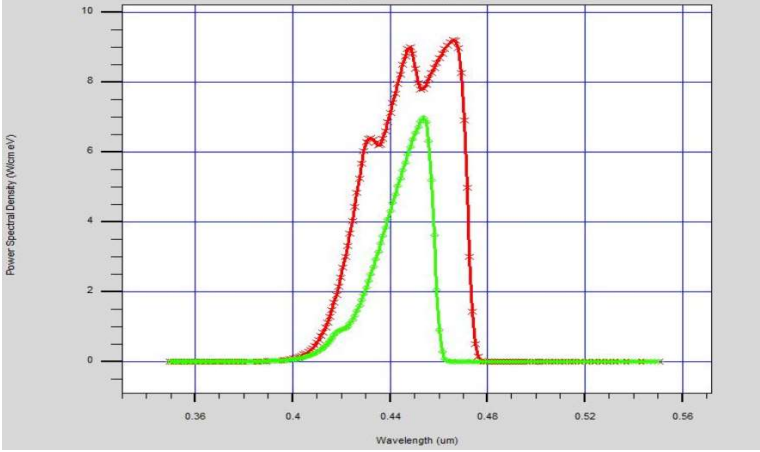

Figure 4.8: Power Spectral Density Curve for 3nm Device at 400K

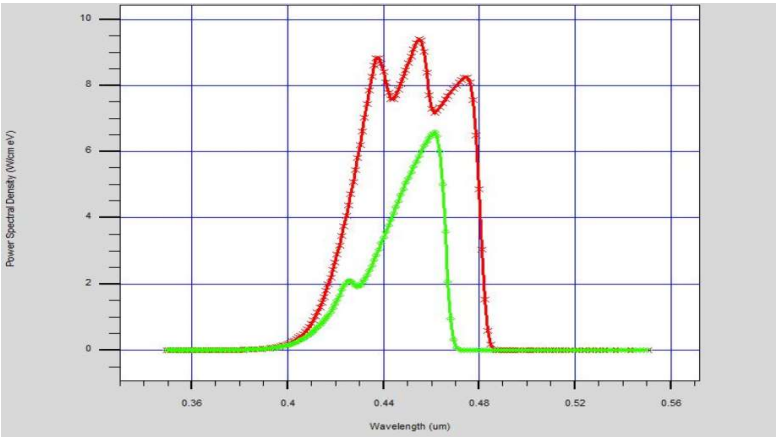

Figure 4.9: Power Spectral Density Curve for 3nm Device at 500K

4.3.2 Power Spectral Density Curves of 6nm Device (Red-Well 2, Green-Well 1)

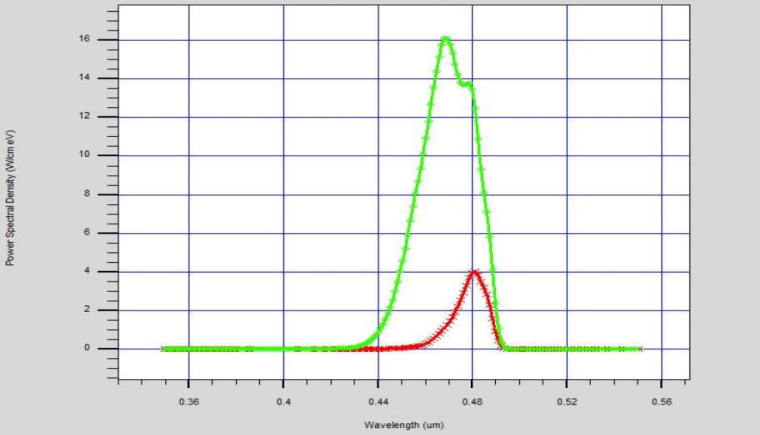

Figure 4.10: Power Spectral Density Curve for 6nm Device at 300K

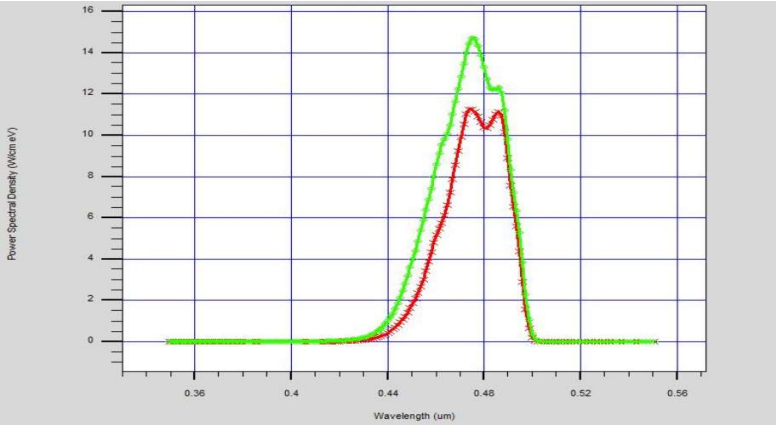

Figure 4.11: Power Spectral Density Curve for 6nm Device at 400K

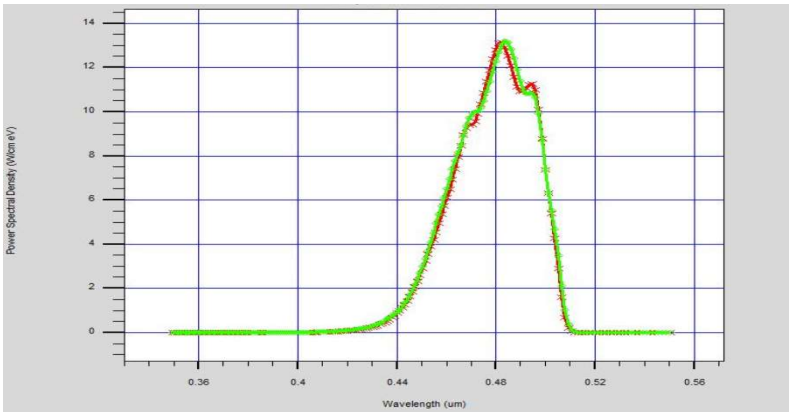

Figure 4.12: Power Spectral Density Curve for 6nm Device at 500K

4.3.3 Power Spectral Density Curves of 9nm Device (Red-Well 2, Green-Well 1)

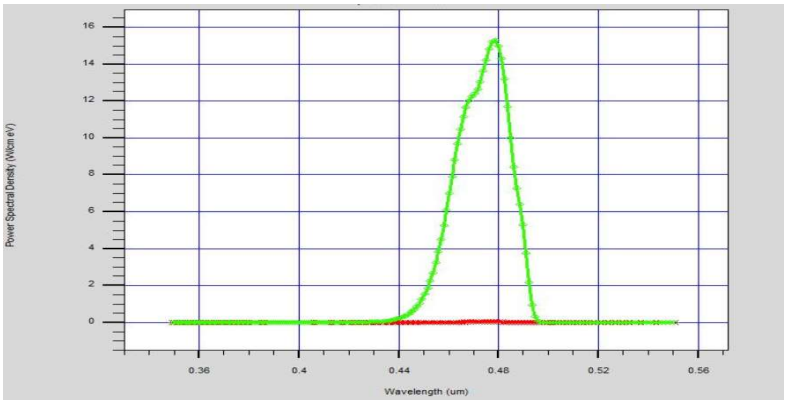

Figure 4.13: Power Spectral Density Curve for 9nm Device at 300K

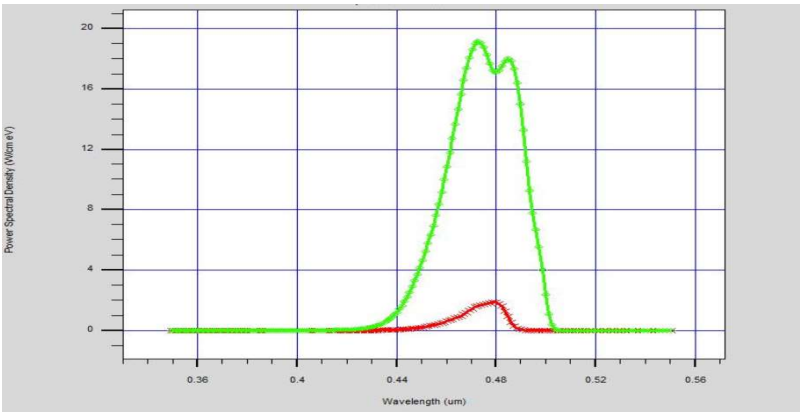

Figure 4.14: Power Spectral Density Curve for 9nm Device at 400K

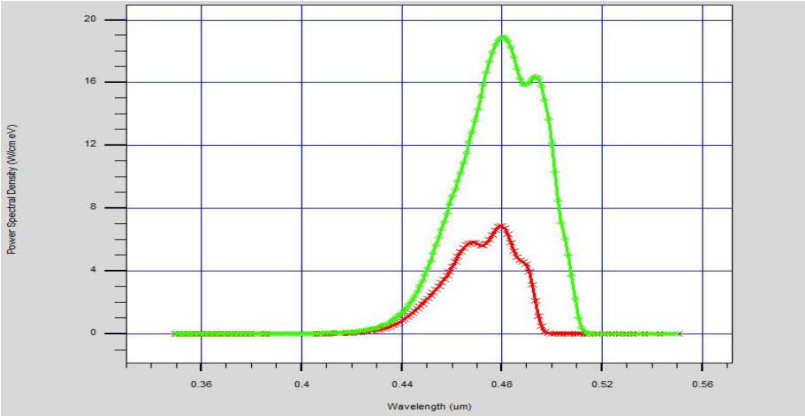

Figure 4.15: Power Spectral Density Curve for 9nm Device at 500K

As the temperature increases to 400K, we can see that Well 1 starts radiating at a higher strength than Well 2 with the formation of shoulders. At 500K, the shoulders of the Red curve became stronger at the lower wavelength side indicating increased radiative recombination from higher energy levels. We suspect that at higher temperatures, electron leakage becomes a big factor where the electrons keep rising to higher bound state energy levels and overflow out of Well 2 (which gets filled with electrons first as it is closer to the "N" doped GaN side).

The dual well structure helps to capture these electrons and cause radiative recombination with holes at higher temperatures which is why we see a boost in PSD of Well 1. This phenomenon is more pronounced in the 6nm wide wells because Well 1 is just about working at 300K. Since Well 2 is wide enough at 6nm it can hold more bound states than 3nm which explains why both the wells were working at good strength in the 3nm device the details we will see later in this paper.

As the temperature rises to 400K and beyond we see Well 1 starting to operate at full strength. This further insinuates to the fact that there is not enough space in Well 2 for electrons and with increased temperature and carriers as we saw before, Well 2

now needs the assistance of Well 1 to increase LOP at high temperature and improve the Internal Quantum Efficiency. The effective volume doubles up at high temperatures which can reduce Auger Recombination.

This is not the case with the 9nm device where Well 1 remains almost inactive all throughout even when subjected to high temperatures. Well 2 being very wide can keep a lot of electrons in its larger number of bound states as we will see from Schrodinger's equation later.

4.4 Variation in Electron Bound Density

Before we jump to electron bound density and how it changes in both the wells that influences the IQE with temperature, we must know about how the electrons get filled up in the quantum wells. The electrons occupy quantized energy levels in the quantum well which is our active region in the LED device. This quantization of energy levels in the quantum wells is derived from the Time Independent Schrodinger equation which is given by equation 4.2

$$\frac{\hbar^2}{2m}\frac{d^2\psi(x)}{dx^2} + \big(E - V(x)\big)\psi(x) = 0 \qquad (4.2)$$

Here $\hbar$ is the reduced Planck's constant, ψ(x) is the wavefunction, m is the effective mass, E is the energy level and V(x) is the barrier potential. On solving the equation, we get 4.3

$$E_n = \frac{n^2\pi^2h^2}{2mL^2} \qquad (4.3)$$

Thus, on solving we get this solution that determines the energy levels in the quantum wells. We see that the width of the quantum well "L" helps to decide the energy difference between the energy levels. Wider the well, smaller is the energy

difference between the quantized levels. We will now use this concept to examine the electron bound density of the three different well structures to understand the variation in PSD and radiative recombination among the wells at different temperatures. The electron bound density is calculated by the square of the electron wavefunction which gives us the probability of finding an electron that is multiplied by the density of states times the Fermi function. The simulation was done in SILVACO for 3nm, 6nm and 9nm wide wells for 300K and 400K to get an understanding of how the electron bound density of the wells were changing that lead to such a trend.

4.4.1 Variation in Electron Bound Density for 3nm device

From the diagrams 4.16 to 4.21 and referring to equation 4.3 we can see that in case of the 3nm device, both the wells have a high electron bound density at 300K which suggests that both the wells are radiating strongly. Since Well 2 is thin at 3nm it will have much higher difference between the energy levels confined in it thus have less number of confined states.

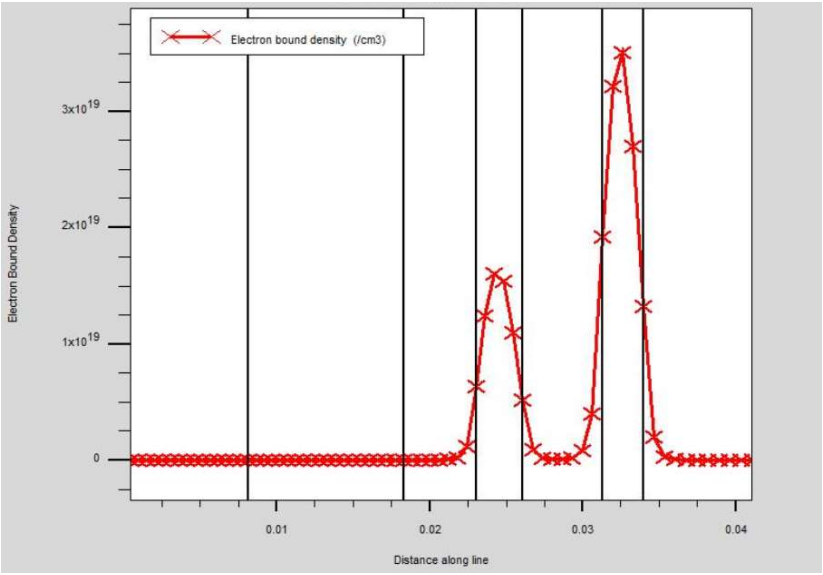

Figure 4.16: Electron Bound Density of 3nm Device at 300K

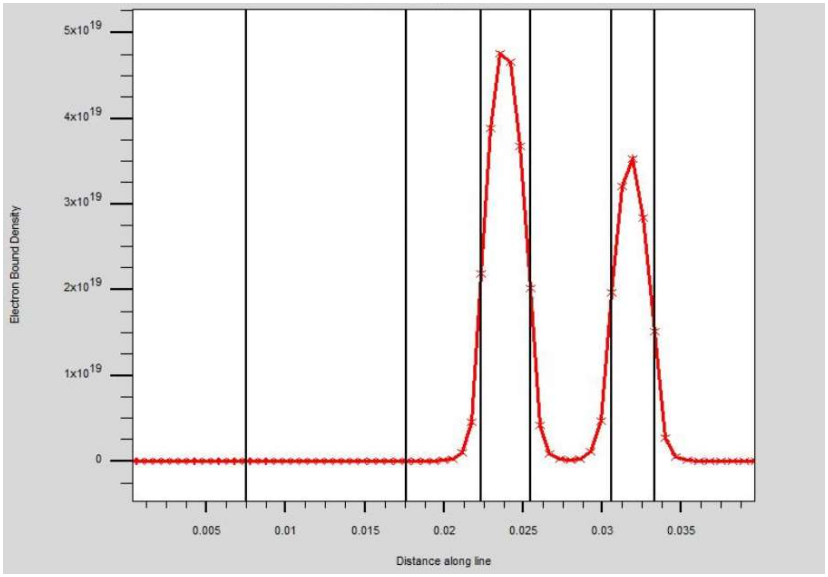

Figure 4.17: Electron Bound Density of 3nm Device at 400K

4.4.2 Variation in Electron Bound Density for 6nm device

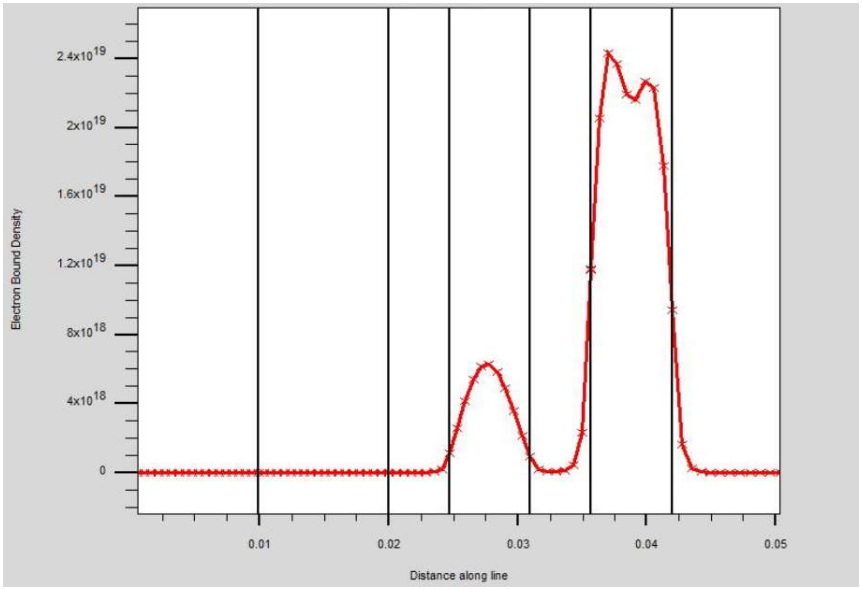

Figure 4.18: Electron Bound Density of 6nm Device at 300K

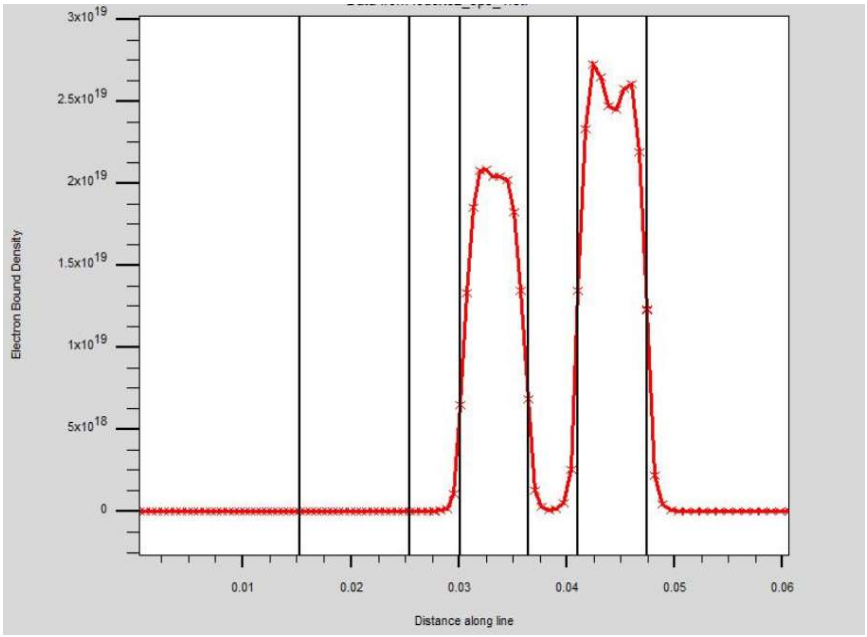

Figure 4.19: Electron Bound Density of 6nm Device at 400K

4.4.3 Variation in Electron Bound Density for 9nm device

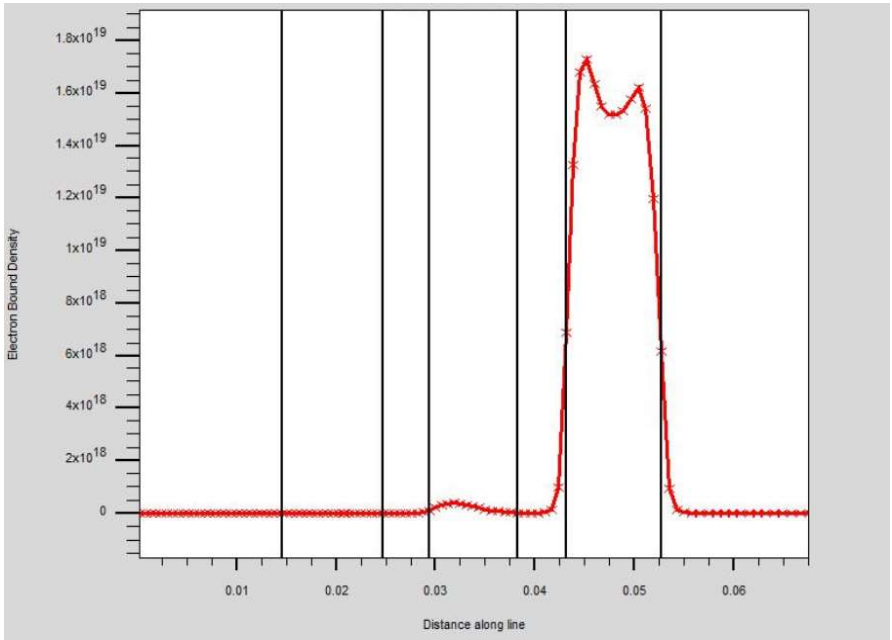

Figure 4.20: Electron Bound Density of 9nm Device at 300K

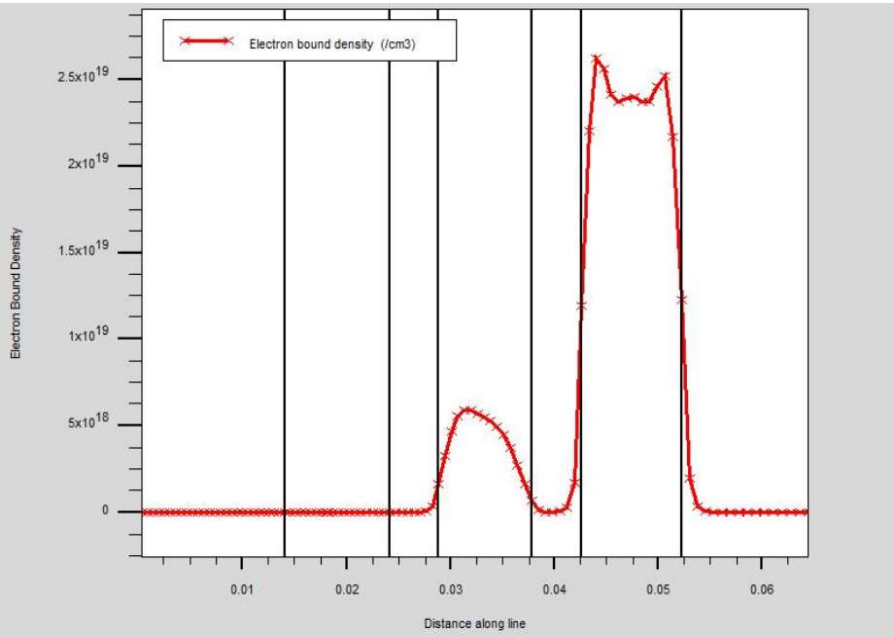

Figure 4.21: Electron Bound Density of 9nm Device at 400K

The excess electrons overflow out of Well 2 even at room temperature. As the temperature is increased it becomes even more difficult for the two thin wells to confine the electrons and thus we have electron leakage as seen in figure 4.22

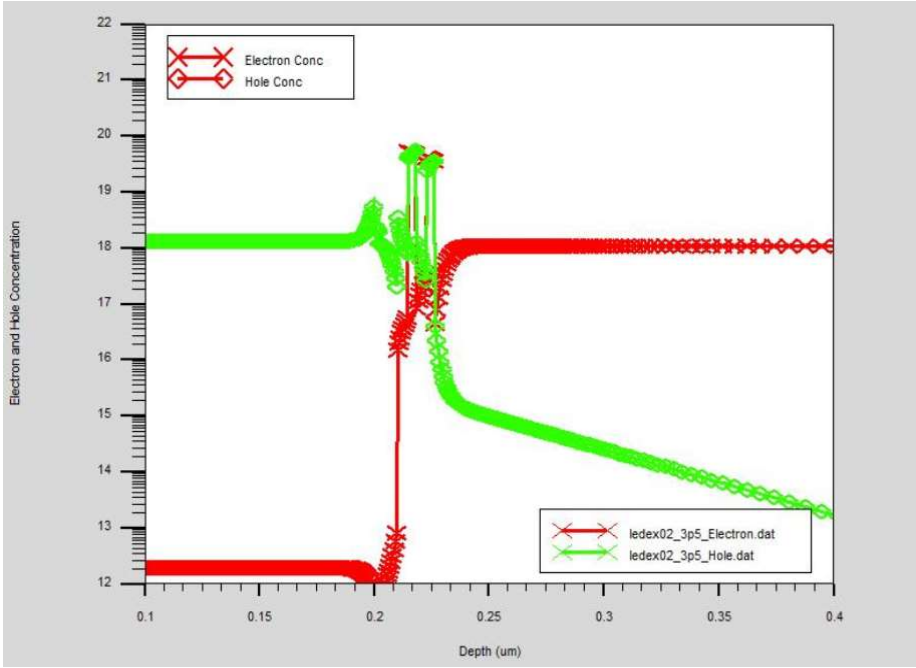

Figure 4.22: Electron and Hole Concentration for 3nm LED Device at 500K

In the 6nm device we can see the electron bound density for Well 1 is much less at 300K suggesting that almost all the radiative recombination is taking place in Well 2 since it is wider and can confine the electrons in it better. As the temperature increases to 400K we can see the electron bound density increase in Well 1 and the PSD shoots up showing strong radiative recombination.

For the 9nm device, since the wells are so wide it can confine all the electrons in it for radiative recombination so we find almost null electron bound density in Well 1 at room temperature.

As the temperature increases, due to the higher number of energy levels in 9nm wells, the electrons just move to higher energy levels with very little moving into Well 1. This phenomenon can be confirmed even further by analysing and comparing the change in percentage overlap of the electron-hole wavefunction overlap among the three devices.

4.5 Variation in Hole Bound Density

Here we have taken the 6nm device and simulated for calculating the hole bound density in both the wells and how it changes as the temperature is changed from 300K to 400K. In Figure 4.23 and 4.24 we can see the graph of hole bound density in both the wells.

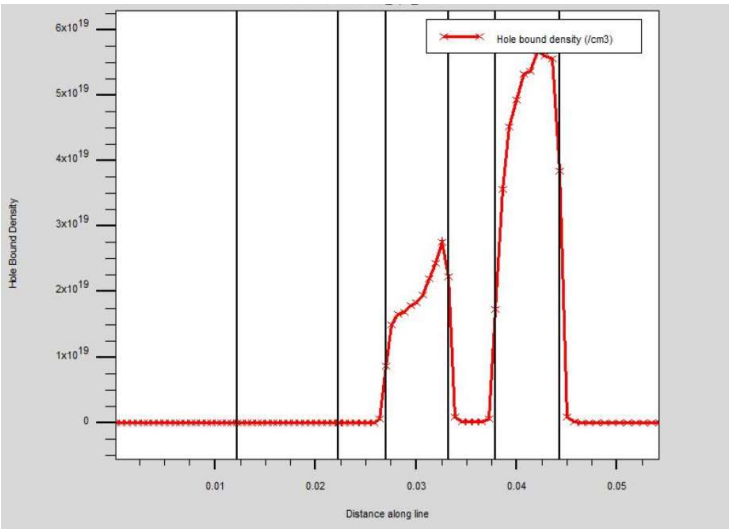

Figure 4.23: Hole Bound Density of 6nm Device at 300K

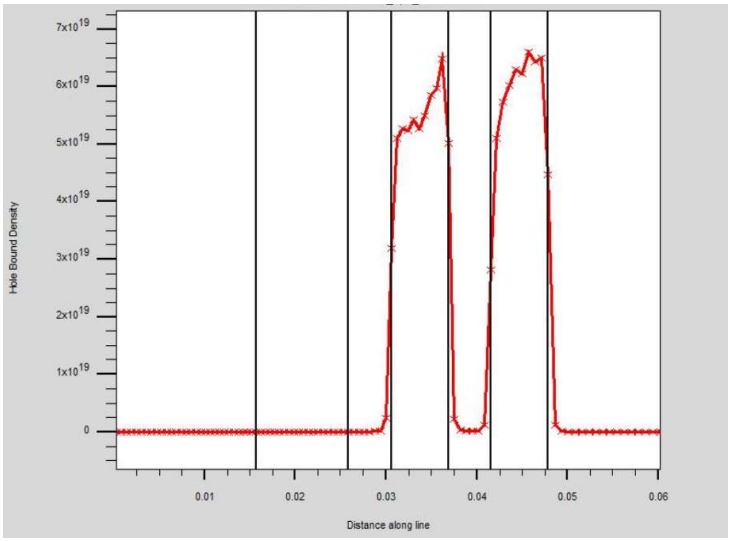

Figure 4.24: Hole Bound Density of 6nm Device at 400K

Here we have an interesting find when we simulate the hole bound density we find that at 300K the peak in Well 1 was only $3e^{19}$ cm^{-3} but as the temperature climbed to 400K it shot up to $6.5e^{19}$ cm^{-3}. We suspect the reduction in bandgap at higher temperatures given by Varshni's equation to be the reason for a consequent reduction in valance band offset leading to increase in hole transport. The Varshni's equation is given by 4.4

$$E(T) = E_0 - \frac{aT^2}{T+b} \tag{4.4}$$

Where E(T) is the bandgap as a function of temperature, T is the temperature in Kelvin, E_0 is the bandgap at 0K, a and b are the material coefficients.

The Conduction band and Valance band of the 6nm device was simulated at 3.5V applied voltage for 300K and 400K and there was an interesting find as we observe from Figure 4.25 and 4.26.

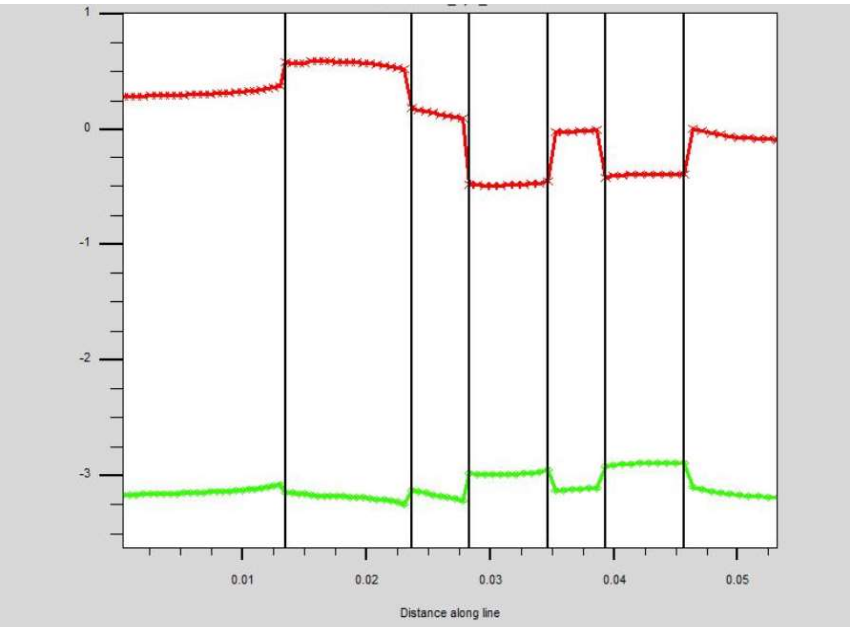

Figure 4.25: Conduction and Valance Band of 6nm Device at 3.5V and 300K

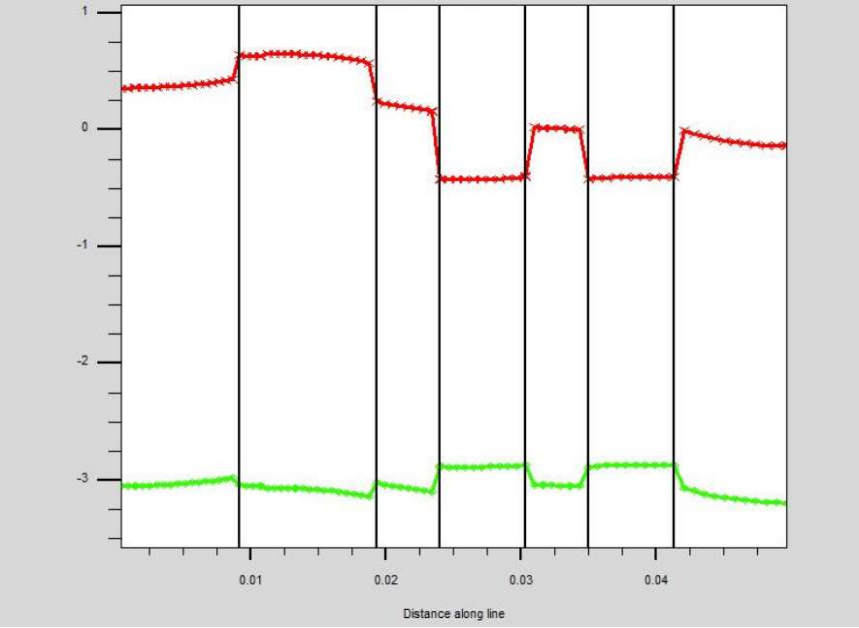

Figure 4.26: Conduction and Valance Band of 6nm Device at 3.5V and 400K

In the two diagrams above we see that the bandgap of the wells reduces as we increase the temperature from 300K to 400K which is also per Varshni's equation, and is also the reason why we see the PSD peaks shift towards longer wavelengths in the PSD graphs.

The interesting thing that we observe here is that if we focus on Well 1 we find that the Conduction band moved up by 0.01eV while the Valance band moved up by 0.104 eV. There was an overall reduction in bandgap which was expected but the change in Valance band energy was large which we believe was caused due to that well, being under strain as it was closer to the AlGaN EBL.

This along with an increase in the number of carriers due to higher temperature and increased electron bound density in Well 1 acted as a magnet for the holes to collect in it and cause strong radiative recombination as we will see with the change in electron-hole wavefunction overlap in the next section.

4.6 Electron-Hole Wavefunction Overlap Change with Temperature

The electron-hole wavefunction overlap was simulated for the three devices for 300K, 400K and 500K. This wavefunction overlap gives us a picture of the probability of interaction of the electrons with holes in the quantum wells.

Increased wavefunction overlap indicates more interaction that insinuates towards increased radiative recombination. The usefulness of the dual well structure at high temperatures is further confirmed by observing the percentage increase in the wavefunction overlap.

The figures 4.27 to 4.29 will show us the variation of wavefunction overlap graph for the 6nm device which is in line with the increase in PSD and carrier bound densities that influences the IQE trend observed before.

4.6.1 Wavefunction Overlap for 6nm Device

The diagrams show an increase in the wavefunction overlap with temperature for the 6nm device in Well 1 which shows the increase in its effectivity with rise in temperature. At very high temperatures even though there is increase in overlap the overall IQE drops due to overflow of electrons from the wells, auger recombination due to high concentration of carriers in a limited volume.

(Electron Bound State Wavefunction Well 1 (Red), Well 2 (Green), Hole Bound State Wavefunction Well 1 (Blue), Well 2 (Cyan))

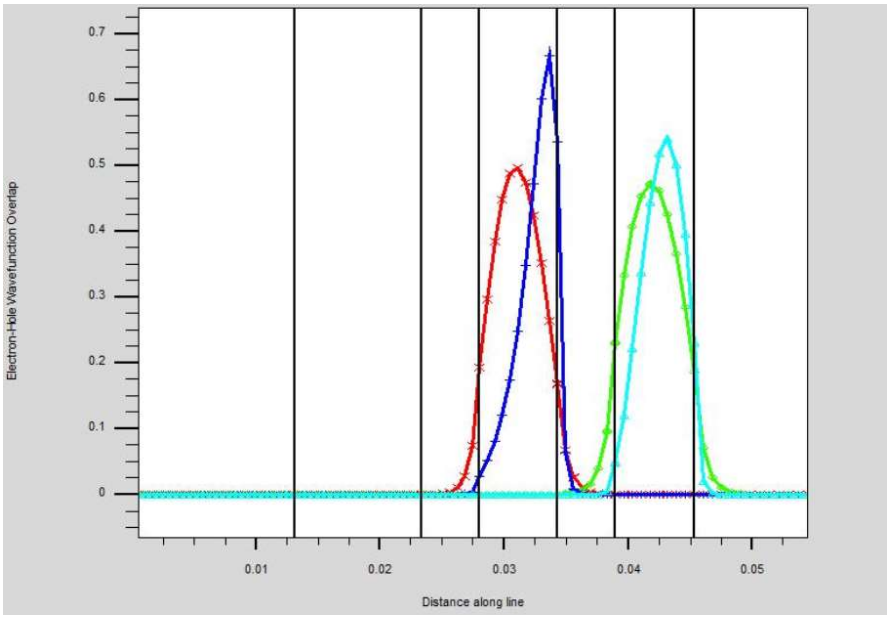

Figure 4.27: Electron-Hole Wavefunction Overlap for 6nm Device at 300K

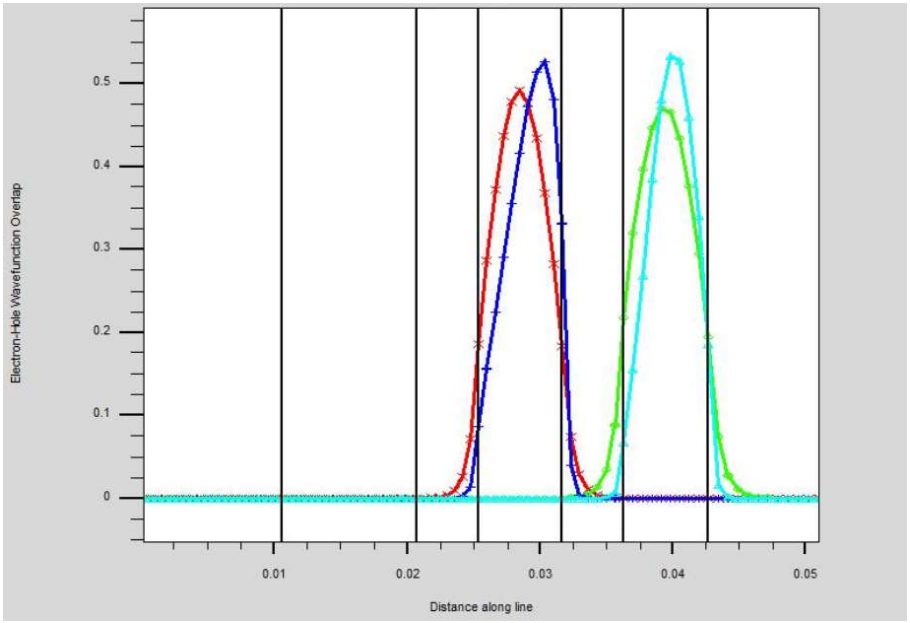

Figure 4.28: Electron-Hole Wavefunction Overlap for 6nm Device at 400K

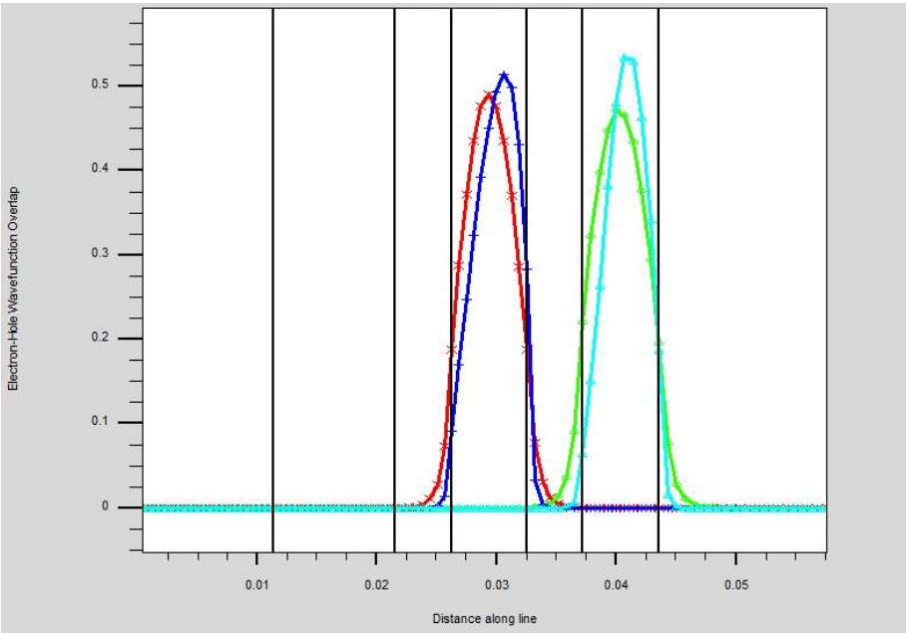

Figure 4.29: Electron-Hole Wavefunction Overlap for 6nm Device at 500K

The Table 4.1 gives us the percentage overlap of the wavefunction overlap that changes with temperature for all three devices that which was calculated by extracting the SILVACO data and coded in MATLAB to find out the percentage overlap area.

Table 4-1: Percentage Overlap of Electron-Hole Wavefunction

	3nm	6nm	9nm
300K	73.45	46.16	9.77
400K	83.19	72.17	18.97
500K	82.46	77.83	35.56

We can see from the PSD, Electron and Hole bound density graphs and the wavefunction overlap data in the table we can see three very different type of behaviour from 3nm, 6nm and 9nm devices. The 3nm device already has both the wells active at room temperature so it is not very effective at higher temperatures.

In the 6nm device Well 1 is almost dormant at room temperature and becomes active at high temperatures thus helping reduce the loss of electrons from high temperature overflow from Well 2 and increasing the effective active region volume to that of both the wells.

This increase in effective volume helps reduce the effect of auger recombination which might influence the Current droop that takes us a bit out of scope of this paper. The problem that the 9nm well suffers from is that Well 1 does not get involved much when we go from 300K to 500K. This can be seen from the wavefunction overlap percentage in Table 4.1.

Since Well 1 does not get involved much in radiative recombination, the effective volume also does not increase by much even when the carrier concentration has increased at higher temperatures. Thus, we find the best performance at 400K is obtained for the 6nm device which hits the sweet spot of operation between 3nm and 9nm devices by utilizing the dual quantum well active region structure properly.

4.7 The complete IQE trend for 6nm Device from 300K to 550K

In figure 4.30, the 6nm wide well device structure was simulated to find out the Internal Quantum Efficiency from 300K to 550K. The temperature was increased in intervals of 25K and the IQE was calculated with respect to anode current.

We observe the IQE improves as the temperature is increased from 300K to 400K where the dual well structure comes to play by activating Well 1. As the temperature increases further, electron leakage becomes stronger, SRH recombination increases, increased carrier concentration and decrease in non-radiative recombination lifetime causes the IQE to go down upwards of 400K.

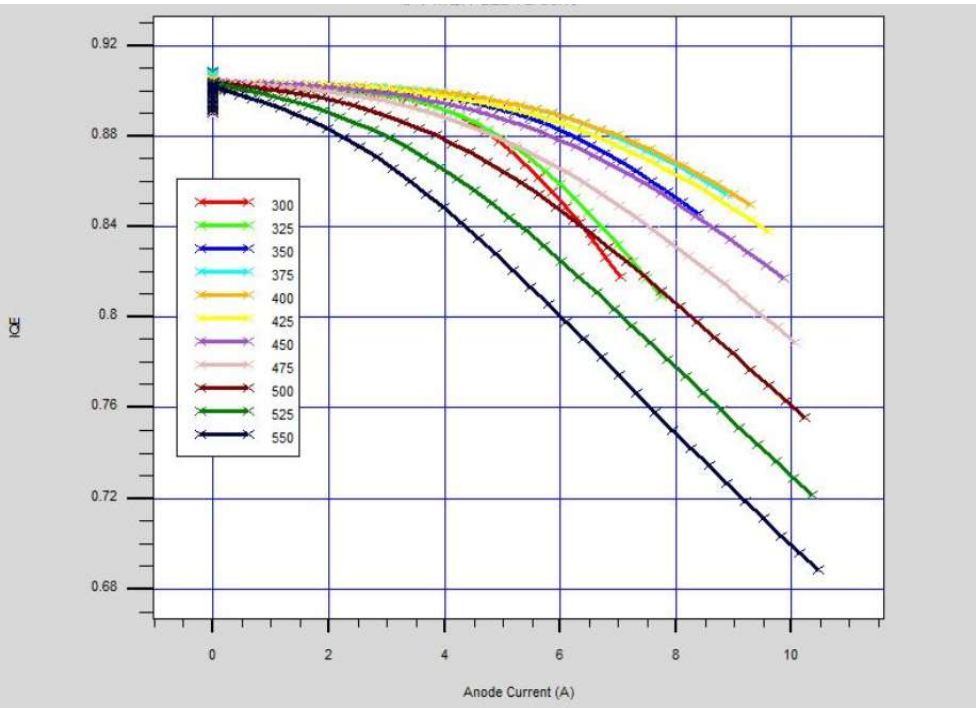

Figure 4.30: Complete IQE Trend for 6nm LED Device from 300K to 550K

Using the equation 1.1, from this graph we can calculate the hot-cold factor and find the hot-cold factor when we move from 300K to 400K is 1.028 for the 6nm device. This value now reduces to 0.99 as we move to 500K at a current injection of 5amps.

CONCLUSION

To conclude, I believe one of the most important invention in the lighting industry was the blue LED. The ability to produce light having energy high up in the spectrum meant it could be used for a large variety of applications. Even with their longer life, robust build and low power consumption, LEDs are plagued by some problems the most significant of which are the current droop and thermal droop. Current droop causes a lowering in the IQE with increased current injection while thermal droop lowers the whole IQE curve with increase in temperature. The focus here was understanding effects of thermal droop and develop a method to control it.

SRH recombination plays a dominant role in the thermal droop effect when the current injection is low. Due to a lower order dependence in the carrier concentration, we find SRH recombination contribute significantly to the reduction in LOP at lower current injection. Since the blue LED is based on GaN, we need to take into consideration the effect of piezoelectric polarization in the quantum wells. The effects of the piezoelectric fields were studied based on the GaN plane orientations.

It was found in a GaN LED simulation study that more the number of quantum wells, lower would be the radiative recombination rate. So, to build the new device structure that would improve LED performance at high temperatures, the initial plan was to build a thick single quantum well design. The shortcoming of a thick single quantum well was the increased spatial separation of the electron and hole wavefunctions that would lead to reduced radiative recombination.

The structure was then developed to be a dual well design where three devices were simulated of 3nm, 6nm and 9nm wide wells. The EBL was reduced in thickness and was made only 10nm thick with a 5nm GaN buffer between it and the active region

wells. The main reason for reducing the EBL thickness was to reduce the valance band offset and improve hole transport into the active region.

The three devices were simulated and the IQE was observed which showed an interesting trend for the 3nm and 6nm devices while it was the same as other devices for the 9nm LED. The PSD, electron bound density and the electron-hole wavefunction data showed the interesting operation of the dual well design. Well 1 which was almost dormant in the 6nm device became active and started radiating when the temperature increased from 300K to 400K. It was found that electrons from Well 2 overflowed out of it and was captured by Well 1 and utilized in useful radiative recombination that lead to an improvement in IQE with rise in temperature. In the 3nm device both the wells were operating at room temperature because of the lower number of energy states present in thin wells. Well 1 did help in assisting Well 2 at higher temperatures which lead to it following a similar trend as the 6nm device. The 6nm device with relatively wider wells, increase the effective volume at higher temperatures and higher carrier concentration as both the wells are being used. This also help reduce auger recombination which improves the IQE.

The 9nm device because of its very wide wells, does not follow the IQE trend like the other two devices because Well 1 is not properly utilized in this design. Well 2 being very wide has the largest number of energy levels which are occupied by electrons. Even with a substantial rise in temperature the electrons do not fill up into Well 1. Thus, the effective volume cannot increase at 400K like in the 6nm device and neither does the radiative recombination rate, leading to decreased IQE.

REFERENCES

[1] S. Nakamura, “Nobel Lecture: Background Story of the Invention of Efficient Blue InGaN Light Emitting Diodes,” in *Nobel Media AB 2014*, 2014.

[2] H. Ou, Y. Ou, A. Argyraki and et. al., “Advances in Wide Bandgap SiC for Optoelectronics,” *Eur. Phys. J. B,* vol. 87: 58, 2014.

[3] D. Meyaard, Q. Shan, E. F. Schubert and e. al., “Temperature dependant efficiency droop in GaInN light-emitting diodes with different current densities,” *Appl. Phys. Lett. ,* vol. 100, no. 8, 2012.

[4] F. Bernardini, V. Fiorentini and D. Vanderbilt, “Spontaneous polarization and piezoelectric constants of III-V nitrides,” *Phys. Rev. B,* vol. 56, no. 16, 1997.

[5] H. Kroemer, “Noble Lecture: Quasielectric Fields and band offsets: teaching electrons new tricks,” 2000.

[6] C.-C. Pan, Y. Zhao, S. Nakamura, S. Tanaka and e. al., “Reduction in Thermal Droop Using Thick Single-Quantum-Well Structure in Semipolar (2012) Blue Light-Emitting Diodes,” *The Japan Society of Applied Physics,* vol. 5, no. 10, 2012.

[7] Q. Dai, Q. Shan, J. Wang and e. al., “Carrier recombination mechanisms and efficiency droop in GaInN/GaN light-emitting diodes,” *Appl Phys, Lett ,* vol. 97, no. 13, 2010.

[8] S. Nakamura , “Shuji Nakamura - Nobel Lecture,” 2014. [Online]. Available: https://www.nobelprize.org/nobel_prizes/physics/laureates/2014/nakamura-lecture-slides.pdf. [Accessed july 2016].

[9] D. S. Meyaard, Q. Shan, Q. Dai and et. al., “On the temperature dependence of electron leakage from the active region of GaInN/GaN light-emitting diodes,” *Apply. Phys, Lett.,* vol. 99, no. 4, 2011.

[10] D. S. Meyaard, Q. Shan, J. Cho and et. al., “Temperature dependent efficiency droop in GaInN light-emitting diodes with different current densities,” *Appl. Phys. Lett.,* vol. 100, no. 8, 2012.

[11] A. Romanov, T. Baker and et. al. , “Strain-inducedpolarization in wurtzite III-nitride semipolar layers,” *Appl. Phys. Lett,* vol. 100, no. 2, pp. 023522-023522.10, 2006.

[12] D. F. Feezell, J. S. Speck, S. Nakamura and et. al., “Semipolar 2021 InGaN/GaNLight-EmittingDiodes forHigh-Efficiency Solid-State Lighting,” *Journal of Display Technology,* vol. 9, no. 4, pp. 190-198, 2013.

[13] K.-T. Lam and S.-J. Chang, “GaN-based LEDs with Hot/Cold factor improved by the Electron Blocking Layer,” *Journal of Display Technology ,* vol. 10, no. 12, 2014.

[14] K.-T. Lam, S.-J. Chang and et. al., “Strain-inducedpolarization in wurtzite III-nitride semipolar layers,” *Journal of Display Technology,* vol. 10, no. 12, pp. 1078-1082, 2014.

[15] J. H. Park, S. Hwang, E. F. Schubert and et. al. , “Enhanced overall efficiency of GaInN-based light-emitting diodes with reduced efficiency droop by Al-composition-graded AlGaN/GaN superlattice electron blocking layer,” *Appl. Phys. Lett,* vol. 103, no. 6, 2013.

[16] J. Chen, G. Fan, w. Pang and et. al., “Comparison of GaN-based light-emitting diodes by using the AlGaN electron-blocking layer and InAlN electron-blocking layer,” *Chin. Phys. Lett,* vol. 28, no. 12, pp. 128501.1-128501.4, 2011.

[17] Y.-Y. Zhang, X.-L. Zhu and et. al. , “Performance Enhancement of Near-UV Light-Emitting Diodes With an InAlN/GaN Superlattice Electron-Blocking Layer,” *IEEE Electron Device Letters,* vol. 33, no. 7, pp. 994-996, 2012.

[18] S. Nakamura, M. Senoh and et. al., “InGaN/GaN/AlGaN-Based Laser Diode Grown on GaN Substrates with a Fundamental Transverse Mode,” *Japanese Journal of Applied Physics ,* vol. 37, no. 2, 1998.

[19] S. Nakamura, M. Sneoh and et. al., “InGaN Multi-Quantum-Well-Structure Laser Diodes with Cleaved Mirror Cavity Facets,” *Japanese Journal of Applied Physics,* vol. 35, no. 2, 1996.

[20] I. Ho and G. Stringfellow, “Solid Phase Immiscibility in GaInN,” *Appl. Phys. Lett,* vol. 69, no. 18, 1996.

[21] J.-Y. Chang and Y.-K. Kuo, “Semiconductor laser and applications,” in *Proc. of SPIE*, Shanghai , 2002.

[22] J.-Y. Chang and Y.-K. Kuo, “Simulation of blue InGaN quantum-well lasers,” *Journal of applied physics,* vol. 93, no. 9, 2003.

[23] Y.-K. Kuo and Y.-A. Chang, “Effects of electronic current overflow and inhomogeneous carrier distribution on InGaN quantum-well laser performance,” *Journal of Quantum Electronics IEEE,* vol. 40, no. 5, pp. 437-444, 2004.

[24] N. Zainal, Z. Hassan, H. A. Hassan and M. Hashim, “Comparative study of single and multiple quantum wells of In0.13Ga0.87N based LED by simulation method,” *Optoelectronics and Advanced Materials - rapid communications ,* vol. 1, no. 8, pp. 404-407, 2007.

[25] Y. Zhao, S. Nakamura and e. al., “Reduction in Thermal droop using Thick Single-Quantum-Well Structure in Semipolar $(20\bar{2}\bar{1})$ Blue Light Emitting Diodes,” *Apply. Phys. Exp,* 2012.

[26] C. Ren, “Polarization fields in III-Nitrides,” *Materials Sience and Technology,* vol. 32, no. 5, pp. 418-433, 2016.

[27] Silvaco,Inc., *Atlas User's Manual,* Santa Clara, California, 2014.

[28] P. Yu and M. Cardona, Fundamentals of Semiconductors: Physics and Materials Properties, Springer, 2005.

[29] D. Vasileska, “K.P method for Electronic Structure Calculation,” [Online]. Available: https://nanohub.org/resources/9455/download/KP_Method_Description.pdf.

[30] J. Dziewior and W. Schmid, “Auger Coefficient for Highly doped and highly excited Silicon,” *Appl. Phys. Lett,* vol. 31, pp. 346-348.

APPENDIX A

SOURCE CODE OF 6NM DUAL WELL LED STRUCTURE

```
go atlas
#Defining the mesh
mesh width=1.13e4
x.mesh loc=0.0   spac=0.5
x.mesh loc=1.0   spac=0.5
y.mesh loc=0.0   spac=0.05
y.mesh loc=0.1   spac=0.001
y.mesh loc=0.2   spac=0.0005
y.mesh loc=0.270 spac=0.001
y.mesh loc=0.285 spac=0.001
y.mesh loc=2 spac=0.10
y.mesh loc=3.285 spac=0.01
#Building the electron blocking layer of the LED device
region number=1 y.max=0.2 material=GaN
region number=2 y.min=0.200 y.max=0.202 material=AlGaN x.comp=0.20
region number=3 y.min=0.202 y.max=0.204 material=AlGaN x.comp=0.20
region number=4 y.min=0.204 y.max=0.206 material=AlGaN x.comp=0.20
region number=5 y.min=0.206 y.max=0.208 material=AlGaN x.comp=0.20
region number=6 y.min=0.208 y.max=0.210 material=AlGaN x.comp=0.20
#Building the active region
region number=7 y.min=0.210 y.max=0.215 material=GaN
region number=8 y.min=0.215 y.max=0.221 material=InGaN x.comp=0.2 name=well
led qwell
region number=9 y.min=0.221 y.max=0.226 material=GaN
region number=10 y.min=0.226 y.max=0.232 material=InGaN x.comp=0.2 name=well
led qwell
region number=11 y.min=0.232 y.max=3.285 material=GaN
```

```
#Setting up the electrodes
electrode name=anode   top
electrode name=cathode bottom
#Setting up the doping of the P regions
doping region=1 uniform p.type conc=5e18
doping region=2 uniform p.type conc=5e18
doping region=3 uniform p.type conc=5e18
doping region=4 uniform p.type conc=5e18
doping region=5 uniform p.type conc=5e18
doping region=6 uniform p.type conc=5e18
#Setting up the doping of the N regions
doping region=11 uniform n.type conc=5e18
#Applying the polarization models
models polarization calc.strain polar.scale=0.15
#Applying the materials parameters
material material=GaN taun0=1e-9 taup0=1e-9 copt=1.1e-8 \
        augn=1.0e-34 augp=1.0e-34
material material=InGaN taun0=1e-9 taup0=1e-9 copt=1.1e-8 \
        augn=1.0e-34 augp=1.0e-34
material material=AlGaN taun0=1e-9 taup0=1e-9 copt=1.1e-8 \
        augn=1.0e-34 augp=1.0e-34

material well.gamma0=10e-3

material edb=0.080 eab=0.101
```

```
#Setting up the LED temperature and applying the device operation models
models temperature=300 k.p fermi incomplete consrh auger optr print
models name=well k.p chuang spontaneous lorentz well.cnbs=4 well.vnbs=4
#Setting up the mobility parameters of the materials
mobility material=GaN fmct.n fmct.p
mobility material=InGaN fmct.n fmct.p
mobility material=AlGaN fmct.n fmct.p
#Output statement
output con.band val.band band.param charge polar.charge e.mobility h.mobility \
      u.srh u.radiative u.auger permi
#Solve statement
solve init
method block newton climit=1e-4 maxtrap=10
solve prev
save outf=led_test_1.str

probe name="Radiative"     integrate radiative rname=well
probe name="Recombination" integrate recombination

log outf=led_test.log
solve vstep=0.1 vfinal=2.5 name=anode
save outf=led_test_2.5.str
save spectrum=led_test_2.5.spc lmin=0.35 lmax=0.55 nsamp=200

solve vstep=0.1 vfinal=3.0 name=anode
save outf=led_test_3.str
```

```
save spectrum= led_test_3.spc lmin=0.35 lmax=0.55 nsamp=200

solve vstep=0.1 vfinal=3.5 name=anode
save outf=led_test_3.5.str
save spectrum= led_test_3.5.spc lmin=0.35 lmax=0.55 nsamp=200

solve vstep=0.1 vfinal=6.0 name=anode
save outf=led_test_6.str

#I-V Curve
tonyplot led_test.log -set ledex02_0.set
# I-L Curve
tonyplot led_test.log -set ledex02_1.set
# EL Spectrum
tonyplot led_test_3.5.spc -set ledex02_2.set

# Extract the Electron and Hole Concentration
extract init infile="led_test_3.5.str"
extract name="Electron" curve(depth,impurity="Electron Conc" material="All" \
      x.val=0.5) outfile="led_test_3.5_Electron.dat"
extract name="Electron" curve(depth,impurity="Hole Conc" material="All" \
      x.val=0.5) outfile="led_test_3.5_Hole.dat"

tonyplot led_test_3.5.str
tonyplot -overlay led_test_3.5_Electron.dat led_test_3.5_Hole.dat -set ledex02_3.set
```